

1 Age and Petrology of the Usun Apau and Linau Balui Volcanics: Windows to Central Borneo's
2 Interior

3 Andrew Cullen*
4 abcullen@hotmail.com
5 Chesapeake Energy
6 Oklahoma City, OK
7 USA
8

9 Colin Macpherson
10 University of Durham
11 Durham, UK

12 Nur Iskandar Taib
13 University of Malaya
14 Kualu Lumpur, Malaysia
15

16 Alex Burton-Johnson
17 University of Durham
18 Durham, UK

19 Dennis Geist
20 Idaho State University
21 Moscow, ID
22 USA

23

24 Terry Spell

25 University Las Vegas

26 Las Vegas, Nevada

27 USA

28

29 Richard Mani Banda

30 Department of Minerals & Geoscience Malaysia,

31 Kuching, Sarawak

32 Malaysia

33

34 ABSTRACT

35 The Usun Apau plateau lies in a remote area of Sarawak along the Tinjar Line, which defines the
36 onshore part of a suture between the Luconia and Dangerous Grounds blocks. Reconnaissance
37 studies in late 1950s established that the plateau is composed of a bimodal suite of young
38 volcanic rocks, but no further work exists to constrain the age and petrogenesis of the Usun Apau
39 Volcanics. We present and discuss new data from a suite of volcanic rocks recently collected
40 from the Usun Apau region. These data include ^{40}Ar - ^{39}Ar age dates of mineral separates, major
41 and trace element geochemistry, and Sr, Nd, Pb isotope geochemistry. The Usun Apau plateau is
42 constructed largely of dacite and andesite erupted between 3.9 to 4.1 Ma. Minor basaltic dikes
43 and flows (*ca.* 2.1 Ma) represent a distinctly younger episode of volcanism that is similar in age
44 and character to the Linau Balui basalts about 100km SE of the plateau. Although the trace
45 element and isotopic suites from both areas indicate the parental melts were generated from a

46 garnet-bearing, LILE-enriched, non-HIMU OIB-like mantle source, depletion in the HREEs and
47 a negative Nb anomaly impart some characteristics of an island arc-type source contribution.
48 The Usun Apau and Linau Balui volcanics are too young to be directly linked to subduction
49 beneath Borneo; indicating a source region possibly modified by an older episode of subduction.
50 Sr, Nd, Pb inter-isotope correlations plot within the same arrays as Pliocene basalts from the
51 Southern Sulu Arc (500 km NE) which suggests much of northern and central Borneo is
52 underlain by similar lithosphere. Assimilation-fractional crystallization modeling indicates that
53 differentiation of the Usun Apau dacite magmas included assimilation of continental crust with
54 very low $^{143}\text{Nd}/^{144}\text{Nd}$. Modeling different basement compositions as contaminants yielded non-
55 unique results. Triassic Malay granite and different Archean granites represent plausible types of
56 assimilants; whereas crust of Dangerous Grounds and Kontum Plateau do not.

57

58 1.0 INTRODUCTION

59 The Usun Apau plateau, one of several volcanic edifices of the interior of Sarawak, separates the
60 headwaters of the Baram and the Pelagus-Rajang rivers (Figures 1 and 2). The plateau is
61 renowned for spectacular waterfalls that spill over its rim; the Julan Falls have a sheer plunge of
62 more than 200m (Hazenbroek and Morshedi, 2001). The plateau averages about 1000m
63 elevation and is constructed of flat-lying volcanic rocks that nonconformably overlie strongly
64 deformed Paleogene flysch of the Rajang-Crocker Group. With annual rainfall on the plateau
65 exceeding 2m (Camerlengo et al. 2000), a youthful age for the plateau is inferred by the
66 preservation of small calderas, which form the Dupoi valley, and constructional cones, such as
67 Bukit Selidang, on the eastern side of the plateau (Figure 2). Campbell (1956) and Kirk (1968)
68 reported the Usun Apau volcanics include hypersthene-bearing dacites cut by subordinate late-
69 stage basaltic dikes. Subsequent studies establishing the age and petrogenetic lineage of the
70 Usun Apau volcanics are lacking, however. Hutchison (2005) noted the need for a modern
71 petrologic and radiometric-dating program targeting the Usun Apau, but expressed doubt that
72 such a program would be undertaken owing to the plateau's remote setting in Borneo's rugged
73 interior highlands. In 2007 a small expedition attempting to climb Bukit Selidang (1373m)
74 collected a suite of samples suitable for the program envisioned by Charles Hutchison. This
75 study reports the analytical results from those samples within the framework of recent studies of
76 Pliocene basalts from the Linau-Balui plateau (Taib, 2012) and the Southern Sulu Arc
77 (Macpherson et al. 2010).

78 2.0 REGIONAL SETTING

79 The lithosphere of the Borneo region comprises several blocks accreted to SE Asia prior
80 to the Cenozoic (Figure 1b; Metcalfee, 2010; Hall, et al. 2009). The SW Borneo Block is a
81 Paleozoic-cored fragment of Australian Gondwanaland sutured to Sundaland during the Middle
82 Cretaceous (Metcalfe, 2010). The greater Dangerous Grounds, which comprises the Luconia, the
83 Dangerous Grounds, and Reed Banks (Figure 1b), collided with the SW Borneo Block along the
84 Lupar Line in the Late Cretaceous (Metcalfe, 2010; Hall, et al. 2009) ending an episode of
85 subduction beneath SW Kalimantan that produced the Schwaner Mountain granites (Hutchison,
86 1996). An interval of relative tectonic quiescence that followed collision of the greater
87 Dangerous Grounds ended with the initiation of SE-directed subduction of the oceanic crust of
88 the proto-South China Sea (ca. 45 Ma; Hall et al. 2009) and ultimately to the progressive
89 collision of the Dangerous Grounds and Reed Banks continental blocks with NW Borneo and
90 Palawan, respectively. The history of subduction of the proto-South China Sea (SCS) beneath
91 NW Borneo is poorly understood. Some workers envision an extensive proto-SCS (Taylor and
92 Hayes, 1983; Hall, 2002; Clift et al. 2008) with protracted subduction that extended into the
93 Early Miocene, whereas Rangin et al. (1999) and Cullen (2010) envision a narrower proto-SCS
94 with less subduction prior to collision of the Dangerous Grounds and Reed Bank with the upper
95 plate of the North Borneo Palawan Block.

96 Hutchison et al. (2000) interpreted the suture between the Dangerous Grounds and North
97 Borneo Palawan Block as passing through the central part of Sabah (Figure 1b). Mesozoic
98 granitic rocks have been dredged from fault scarps on the Dangerous Grounds (Kudrass et
99 al.1986; Yan et al. 2010). Zircons from the Late Miocene Mt. Kinabalu pluton with inherited
100 Late Cretaceous and older cores (Cottam et al. 2010) are strong evidence that Dangerous
101 Grounds basement extends to the suture proposed by Hutchison et al. (2000). Although the

102 North Borneo Palawan Block has an oceanic character marked by exposures of Lower
103 Cretaceous ophiolites, the nature of the basement supporting the Sabah and South Palawan
104 ophiolites is unclear. Several lines of evidence suggest this basement is of a continental affinity;
105 Jurassic to Triassic age granitoids crop out in small windows beneath the ophiolites (Hutchison,
106 2005), Pliocene basalts from the Southern Sulu Arc have isotopic signatures indicating
107 assimilation of Archean continental crust (Macpherson et al. 2010), Bouguer gravity data
108 indicate that most of Sabah is underlain by low density crust (Milsom and Holt, 2001), and to the
109 NE the Sulu Sea and Palawan have been interpreted as part of micro-continental plate (Bird et
110 al. 1993; Yumul et al. 2009).

111 The Usun Apau plateau lies along the Tinjar Line where a deflection in the structural
112 grain of the underlying Rajang-Crocker Group defines a large oroclinal bend (Figure 1a;
113 Hutchison, 2010). The Tinjar Line is often shown extending offshore extension to link with the
114 West Baram Line (Figures 1 and 3). These “lines” are poorly understood features that have never
115 been rigorously defined. In early tectonic models (Hamilton, 1978; Hollaway; 1982; Daly et al.
116 1991) the lines are not featured; whereas some subsequent models interpret these lines as lying
117 along a transform boundary that accommodated differential motion between the Luconia Block
118 and the Dangerous Grounds during subduction of the proto-SCS (Figure 1b; Morley, 2002; Clift
119 et al. 2006; Hall, et al. 2009). With respect to current plate boundaries, however, the Usun Apau
120 plateau represents an intra-plate tectonic setting that is ideally located to study the nature of the
121 Luconia Block in relation Borneo’s other possible basement fragments. To the extent that
122 volcanic rocks represent direct, albeit modified, samples of the lower crust and upper mantle, the
123 distribution, age, and composition of Borneo’s igneous rocks provide information with which to
124 constrain models for the region’s tectonic evolution. Borneo’s Cenozoic igneous record is

125 intriguing and somewhat problematic. Igneous rocks of various ages, although widespread, are
126 limited and not a volumetrically significant portion of the rock record. Episodes of bimodal
127 volcanism that occurred in the Late Eocene and Late Miocene to Pleistocene are separated by
128 Oligocene-Miocene calc-alkaline igneous activity. For the purposes of this paper we group
129 Borneo's Cenozoic igneous rocks into 5 informal units (Figure 3).

130 1. The Usun Apau and Linau Balui plateaus belong to a group of dissected Plio-Pleistocene
131 volcanic tablelands that cap parts of Borneo's interior highlands. These tablelands include the
132 Nieuwenhuis Mountains, and the Nankan plateau, and thus mostly lie SW of the Tinjar line
133 (Figure 3). Owing to their remote location, the volcanic rocks of tablelands remain relatively
134 under-studied. Basalts, dacites, and andesites have been reported (reviewed by Tate, 2002;
135 Hutchison, 2006) and a limited number of age determinations indicate Pliocene to
136 Pleistocene magmatic activity (Weerd and Armin, 1992).

137 2. The Southern Sulu Arc (SSA) comprises Early to Middle Miocene andesites, which record
138 short-lived subduction of part of the Celebes Sea beneath SE Sabah, as well as Plio-
139 Pleistocene basaltic rocks that post-date subduction (Chiang, 2002; Hutchison, 2005). Those
140 basalts have been interpreted as being derived by partial melting of from an OIB-like mantle,
141 and some of the more evolved basaltic andesites have radiogenic isotopic ratios indicative of
142 assimilation of ancient continental crust basement. (Macpherson et al. 2010).

143 3. The Sintang suite is represented primarily by Oligocene to Miocene calc-alkaline stocks,
144 plugs, and dikes (Van Bemmelen, 1949; Soeria-Atmadja, 1999) that are associated with
145 epithermal gold mineralization (van Leeuwen, et al. 1990). The Sintang suite occurs mostly
146 in Kalimantan, but extends into Sarawak, Malaysia, near the city of Kuching where two
147 distinct phases of igneous activity are recorded; Early Miocene (23.7 Ma to 23.3 Ma) calc-

148 alkaline diorites and Middle to Late Miocene (14.6 Ma to 6.4 Ma) microtonalites and dacites,
149 which have an adakite signature (Prouteau et al. 2001). The Kuching adakites are associated
150 with gold-antimony mineralization and have been interpreted as re-melting of oceanic
151 lithosphere modified during an earlier episode of subduction (Prouteau et al. 2001).
152 Alternatively, the Linhaisai minettes (*ca.* 8 Ma, ultra-potassic phlogopite-bearing mafic
153 dikes) in the Central Kalimantan (Figure 3) suggests the region is underlain by enriched
154 subcontinental mantle lithosphere (Bergman et al. 1988).

155 4. Mt. Kinabalu is an isolated, sheeted, granitic pluton in northern Sabah, Malaysia, that was
156 emplaced in several short pulses between 7 and 8 Ma (Cottam et al. 2010); it can be regarded as
157 post-dating subduction and collision of Dangerous Grounds continental crust. Isotopic data
158 show that older pulses have more radiogenic Sr and Pb and less radiogenic Nd and Hf than
159 the younger pulses, which may reflect either differences in crustal assimilation or
160 incongruent dehydration melting of a sole source (Burton-Johnson and Macpherson, 2012).
161 Inherited zircon ages from the Mt. Kinabalu pluton indicate it is underlain by subducted
162 Mesozoic Dangerous Grounds continental crust (Cottam et al. 2010).

163 5. Bi-modal Eocene volcanic rocks crop out at several widely separated locations (Pieters and
164 Supriatna, 1990) and have been penetrated by exploration wells in nearly all of Kalimantan's
165 onshore basins (Satyana et al. 1995). This episode of volcanism is likely related to the early
166 rift phase of basinal extension (Hutchison, 1996). The Bukit Mersing basalts, approximately
167 100 km east of the Linau Balui plateau (Figure 3), have trace element characteristics of ocean
168 island basalts (Taib, 2006). These basalts are important because their geochemical signature
169 predates any modification of the lithosphere during Oligocene-Early Miocene tectonism.

170 3.0 FIELD PROGRAM & SAMPLING

171 The Usun Apau plateau covers an area of about 770 km². Its original extent, although
172 undoubtedly larger, is not known. The plateau's margins are steep; sheer drops up to 300m
173 reflect the thickness of the lavas and welded tuffs that make up the plateau and cap steeply
174 dipping sandstones and shales of the Belaga Formation. Fresh outcrops are limited to stream
175 cuts in deep ravines. Access is limited and dangerous. Because high runoff and strong currents
176 quickly round material transported from the plateau and remove weathering rinds, river cobbles
177 collected near the base of the plateau provide fresh, albeit out of place, samples. Owing to the
178 relatively small size of the plateau and numerous drainages the river cobbles represent samples
179 transported only short distances. On the south side of the plateau, 8km from Bukit Selideng, the
180 seven UP samples were collected from the Silio River near the base of the Silio Falls (Figure 2)
181 where crudely bedded welded tuffs overlie weakly jointed lava flows (Figure 4). In hand sample
182 the welded tuffs have well developed flow banding defined by black fiamme; UP4 had visible
183 quartz and was classified as dacite. The lavas, 15% plagioclase phenocrysts set in an aphanitic
184 groundmass, were classified in the field as andesite owing to their light gray color. Additional
185 samples from Usun Apau caldera walls and from Linau-Balui plateau were collected during field
186 work between 1982 and 1987 (Banda and Aji, 2012) and analyzed by Taib (2012).

187 4.0 ANALYTICAL METHODS

188 Appendix A summarizes our analytical techniques and results are given in Tables 1, 2
189 and 3. Age determinations used performed using the Ar-Ar method (University of Nevada Las
190 Vegas), major and trace elements were measured by X-ray Fluorescence Spectroscopy
191 (Washington State University and University of Malaya); and trace elements and radiogenic
192 isotopes were measured by Inductively Coupled Plasma Mass Spectrometry (Washington State
193 University, Vrij University Amsterdam, and Durham University).

194

195 5.0 RESULTS

196 5.1 Petrography: Examination of standard, but unstained, thin sections confirmed the
197 field classifications of andesite and welded tuff (Figure 5). The welded tuffs have a glassy
198 groundmass with numerous small opaque crystals presumed to be Fe-Ti oxides. Euhedral to
199 subhedral hypersthene phenocrysts set in the groundmass suggest pyroxene was an equilibrium
200 phase at the time of eruption. Plagioclase phenocrysts (*ca.* An₄₀ from extinction angles) are also
201 present; some show strong oscillatory zoning indicative of minor fluctuations in the magma
202 chamber prior to eruption (Figure 5c). Groundmass plagioclase is slightly more sodic (*ca.* An₃₀).
203 Although rare, small grains of biotite are present; these yielded reliable age dates. Several
204 samples have large anhedral quartz grains with highly embayed rims around which the glassy
205 groundmass shows viscous flow features (Figure 5a). Abundant inclusions of rutile are present
206 in some quartz grains indicating a plutonic source (Figure 5b). The Usun Apau plateau is
207 constructed upon a thick section of the Belaga Formation which has sandstones derived largely
208 from a granitic provenance such as the Schwaner Mountains (van Hattum et al. 2006). We
209 interpret the quartz grains as xenocrysts from the Belaga Formation, rather than an equilibrium
210 phase at the time of eruption. The lava flows have a pilotaxitic texture owing to alignment of
211 plagioclase laths (*ca.* An₄₀) and subhedral hypersthene (Figure 5d). The phenocrysts in the lavas
212 are smaller than those in the welded tuffs. Rounded quartz grains are present, but rare, whereas
213 biotite was not seen in thin section.

214 5.2 ³⁹Ar-⁴⁰Ar Age Determinations: Three samples were analyzed using conventional
215 furnace step-wise heating analyses on bulk mineral separates (Table 1). Although the samples
216 had U-shaped age spectra commonly associated with excess argon (Figure 6), stable plateau ages

217 could be determined for each sample; UP 7 yielded a 3 point isochron age. An isochron age is
218 the best estimate of the age of a sample, even if a plateau age is obtained.

219 The age spectrum for the UP-4 biotite is characterized by high initial ages (step 2 ~6.2
220 Ma) that decrease progressively to ages of ~4 Ma by ~10% gas released. This decline is
221 followed by a flat, concordant age spectrum for the remainder of the gas released. The total gas
222 age, which is equivalent to a conventional K/Ar age, is 3.96 ± 0.03 Ma. Steps 8-13 (77% of the
223 ^{39}Ar released) define a slightly younger, but statistically indistinguishable, plateau age of $3.90 \pm$
224 0.04 Ma. There is no isochron defined by these data. Ca/K ratios are slightly high in the first
225 few steps, but otherwise generally consistent with outgassing of a homogeneous biotite mineral
226 separate. Radiogenic yields ($\%^{40}\text{Ar}^*$) are somewhat low for a high-K phase of this age, which
227 may indicate some alteration is present. The high initial ages are likely caused by recoil of
228 reactor-generated ^{39}Ar out of the biotite crystals, which based on $\%^{40}\text{Ar}^*$ could contain chlorite
229 intergrowths that would result in a depleted layer near the surface of the crystals, the first
230 material to outgas on step heating. Thus, initial ages from recoil affected samples are
231 anomalously high. The possibility that the shape of this age spectrum is a result of excess argon
232 in the sample cannot be confirmed, as no isochron is defined by these data. The overall
233 concordant nature of the age spectrum and the observation that recoil artifacts are common in
234 biotites, the plateau age (3.90 ± 0.04 Ma) is considered the most reliable for this sample.

235 The UP-8 biotite sample produced an age spectrum similar to the UP-4 biotite and is
236 interpreted similarly. The total gas age for this sample is 3.94 ± 0.04 Ma. Steps 6-10 (69% of
237 the ^{39}Ar released) define a slightly younger (statistically indistinguishable) plateau age of $3.86 \pm$
238 0.05 Ma. Steps 6-8 (57% of the ^{39}Ar released) define a statistically valid isochron, which yields

239 an age of 3.84 ± 0.06 Ma and an initial $^{40}\text{Ar}/^{36}\text{Ar}$ ratio of 301.0 ± 4.5 , indistinguishable from
240 atmospheric argon at the 2σ uncertainty level. Although the isochron is defined by only 3 points,
241 it is important that the isochron does not suggest excess argon is present. Ca/K ratios are
242 initially high, and again with the final step, suggesting the presence of another mineral phase in
243 this biotite separate. The affected steps account for $\sim 12\%$ of the total gas released. Radiogenic
244 yields are somewhat low, suggesting some alteration may be present. Although all 3 ages are
245 identical within 2σ uncertainties, the plateau age (3.86 ± 0.05 Ma) is considered the most reliable
246 for this sample.

247 UP-7, a plagioclase separate, is characterized by a discordant age spectrum with high
248 initial age of ~ 5.7 Ma, followed by steps of progressively decreasing age until step 7 (4.11 ± 0.07
249 Ma), and then progressively increasing ages to a final step at 7.1 Ma. The total gas age is $5.11 \pm$
250 0.05 Ma. There are no plateau or isochron ages defined by these data. Ca/K ratios are somewhat
251 low and varied for a plagioclase, unless this is a very high-K plagioclase which is not consistent
252 with petrographic observations. Radiogenic yields are as expected for a plagioclase of this age.
253 However, the very low radiogenic yields in the final steps, which are generally of higher
254 radiogenic yield, suggest some alteration of the mineral separate. The form of the age spectrum
255 is distinctly U-shaped, suggesting excess argon is present, although this cannot be confirmed via
256 an isochron. The most conservative interpretation in this case is to assume excess argon is
257 present, and thus the youngest age on the age spectrum (step 7, 4.11 ± 0.07 Ma) is a maximum
258 age for the sample. The age Ar-Ar age dates are consistent with outcrop observations at Silo
259 Falls that welded tuffs (UP-4, 3.90 ± 0.04 Ma and UP-8, 3.84 ± 0.06 Ma) overlie lava flows
260 (4.11 ± 0.07 Ma). Preliminary dating of a basalt from the Usun Apau plateau yields an Ar-Ar

261 age of 2.0-2.5 Ma (Taib, 2012) similar to the age of the basalts from the Linau Balui plateau
262 (Taib, 2012).

263 5.3 Major and Trace Element Geochemistry: Table 2 summarizes the major and trace
264 element analyses. Our sample set represents widespread coverage, albeit from a limited number
265 of locations. Considering the difficult access to the interior highlands, this sample set must serve
266 as a representative suite until future expeditions sample other areas. Samples from the Silio Falls
267 on the southeastern side of the plateau present an excellent vertical succession. The Silio Falls
268 samples straddle the dacite and andesite boundary on a plot of $\text{Na}_2\text{O}+\text{K}_2\text{O}$ vs. SiO_2 and are
269 similar to the adakites of the Sintang suite near Kuching (Figure 7). Two dacite samples from
270 the northern area around Bukit Mabun (Figure 2) analyzed by Kirk (1957) are relatively enriched
271 in the alkalis and plot in the trachyte field (Figure 7). The late-stage basalt to basaltic andesite
272 dikes from the Usun Apau plot with the Linau Balui basalts (Figure 7; Taib, 2012). The major
273 and trace element abundances vs. SiO_2 show the distinct groupings for samples from the different
274 areas of the Usun Apau plateau; however intra-area compositional differences are narrow
275 (Figures 8a and 8b). For example, UP81, higher in silica and presumably more evolved, is
276 depleted in Zr relative to the Silo Falls dacites (Figure 8b). Samples from Bukit Mabun on the
277 northern side of the plateau are enriched in alkalis, but depleted in magnesium, relative to the
278 Silio Falls dacites (Figure 8a). An andesite (TN96) from the Tinjar area has elevated Rb, but low
279 Zr concentrations, which imparts a unique signature relative to other samples (Figure 8b). All
280 samples have relatively low Nb, Sc, and Y concentrations (Figure 8b).

281 The N-MORB normalized multi-element plots for the Linau Balui and Usun Apau
282 samples show enrichment in large-ion-lithophile elements (LILE) and depletion in the high-field
283 strength elements (HFSE) and the heavy rare earth elements (HREE); UA43 shows very strong

284 enrichment in LILE relative OIB (Figure 9). The Usun Apau basalts are more enriched in LILE
285 the Linau Balui basalts; both are enriched in LILE relative to OIB. The more evolved samples
286 show much stronger LILE enrichment, but similar depletion in HFSE and HREE. All samples
287 show strong relative depletion in Nb and a modest positive Zr anomaly relative to Ti; the Usun
288 Apau dacites show very strong depletion in Ti. Although such negative anomalies are commonly
289 associated with island arc tholeites, the steep LILE to Nb trend is largely a reflection of LILE
290 enrichment. Only two samples (UA43 and TN96) have $(\text{La/Nb})_n$ ratios >1 , although generally an
291 indicator of a subduction signal, crustal contamination cannot be excluded. Overall, the volcanic
292 rocks from both plateaus appear to be derived from a similar LILE-enriched OIB-like mantle
293 source.

294 5.4 Isotope Geochemistry: The Usun Apau and Linau Balui samples display wide ranges
295 in their radiogenic isotopic ratios, $^{87}\text{Sr}/^{86}\text{Sr}$, $^{143}\text{Nd}/^{144}\text{Nd}$, $^{206}\text{Pb}/^{204}\text{Pb}$, $^{207}\text{Pb}/^{204}\text{Pb}$, and $^{208}\text{Pb}/^{204}\text{Pb}$
296 (Figures 10 and 11; Table 3). Both sample suites show trends towards higher $^{87}\text{Sr}/^{86}\text{Sr}$ and
297 lower $^{143}\text{Nd}/^{144}\text{Nd}$ as a function of SiO_2 (Figure 10). Because such isotopic variations should not
298 occur during fractional crystallization of magmas derived from similar source regions, the
299 observed trends strongly indicate assimilation played a role in their differentiation, particularly
300 the Usun Apau dacites. Strong inter-isotope correlations for the Usun Apau and Linau Balui
301 volcanics define arrays similar to those of the SSA basalts (Figure 11), which have been
302 interpreted as the result of fractional crystallization coupled with assimilation of continental crust
303 (Macpherson et al. 2010).

304 6.0 DISCUSSION

305 Our study of the volcanic rocks from the Usun Apau and Linau Balui areas reveals
306 important information regarding a previously unknown part of central Borneo and fills an
307 important data gap between the southern Sulu Arc and the Sintang Intrusives near Kuching.
308 Specifically, we are able to address five important considerations: (1) age of magmatic activity,
309 (2) nature of their source regions, (3) the nature of the subsurface crust via melt-crust interaction,
310 (4) the relationship of Luconia to other crustal blocks, and (5) causes of volcanism.

311 *6.1 Episodes of Volcanic Activity:* The Usun Apau plateau records two short-lived
312 episodes of volcanism. Eruption of andesitic to dacitic lavas and tuffs (4.11 ± 0.07 Ma and 3.90
313 ± 0.04 Ma), which form most of the plateau, was followed by a period of quiescence that ended
314 with a very small volume of basaltic volcanism (*ca.* 2.0 Ma). The N-S alignment of light-
315 colored elliptical tonal anomalies on the NE edge of the plateau (Figure 2, inset) may indicate
316 recent geothermal activity. Although the basalts and more evolved rocks appear to form
317 relatively coherent differentiation arrays (Figures 7 and 8a), several lines of evidence lead us to
318 interpret these as two distinct magmatic episodes rather than eruption from a single stratified
319 magma chamber. First and foremost, the more evolved rocks are distinctly older than the basalts.
320 The similar timing of basaltic volcanism at the Usun Apau, Linau Balui, and Nankan plateaus
321 (Figure 3) suggests that this activity is related to a younger more widespread episode. Moreover,
322 several incompatible trace elements have trends opposite that predicted from fractional
323 crystallization. For example, Nb decreases with decreasing MgO through the spectrum of basalt
324 to dacite with different ages, but stays relatively constant within each suite (Figure 12a). For the
325 Linau Balui basalts K/Nb, which should be relatively invariant, decreases with MgO (Figure
326 12a). We interpret Usun Apau volcanism as pulsed sampling of a single mantle source at *ca.* 4
327 and *ca.* 2 Ma. The earlier silicic phase of magmatism, more enriched in incompatible trace

328 elements (Figure 9), supplied a larger volume of melt to the surface producing an andesitic
329 plateau capped by welded tuffs. The evolved character of this magmatism suggests that there was
330 a period of prolonged differentiation at crustal levels. Basalts of the later phase did not
331 experience a similar extent of differentiation, so may have ascended more rapidly to the surface.

332 6.2 *Nature of Source Region*: The basaltic rocks from Usun Apau and Linau Balui
333 provide the best estimate of the nature of their mantle sources. The least evolved rocks show
334 relatively smooth normalized trace element patterns that indicate an LILE-enriched OIB-like
335 mantle region (Figure 9). Depletion of the heavy rare earth elements in the Usun Apau and
336 Linau Balui volcanics indicates the presence of garnet and/or amphibole in the source region.
337 Relative to the amphibole-bearing Kuching adakites, the Usun Apau dacites are enriched in Rb
338 (Figure 12c), but have a lower K/Rb (Figure 12d). The presence of pyroxene rather than
339 amphibole as a phenocryst phase in the Usun Apau dacites coupled with their lower K/Rb ratios
340 likely reflects the absence of buffering by amphibole, which preferentially retains Rb. The low
341 concentrations of Ti and Nb (Figures 8 and 9) point to either rutile and/or ilmenite in the source
342 region, or enrichment by metasomatic fluids depleted in the relatively insoluble HSFES. The
343 absence of a negative Eu anomaly (Figure 9) and mildly elevated Sr/Y in the dacites (Figure 12b)
344 are interpreted to reflect the lack of extensive plagioclase fractionation and/or its absence in the
345 source region. Considering the stability fields for garnet, plagioclase, and amphibole (Green and
346 Falloon, 2005; Stern, 2002), the trace element data suggest Usun Apau and Linau Balui parent
347 magmas were derived from depths of at least 60km to 80km. The fact that the Usun Apau
348 volcanics have an average Cr/Ni ratio (1.84) similar to that for primitive mantle, suggests
349 equilibration of melt in the presence of mantle peridotite (Yogodzinski et al. 1995; Raap et al.
350 1999).

351 With the exception of UA43, a basalt, which stands out as anomalous, the MORB-
352 normalized trace element data for the Linau Balui basalts, the Usun Apau basalts, and the Usun
353 Apau dacites plot in sufficiently tight groupings that we have plotted the average for these
354 groups along with trace element data from other areas (Figure 13). The Linau Balui and Usun
355 Apau basalts resemble the Plio-Pleistocene basalts of the SSA, which suggests that the Usun
356 Apau and Linau Balui basalts are derived from a mantle source similar to that invoked for
357 Southern Sulu Arc by Macpherson et al. (2010). Higher LILE contents in Usun Apau volcanics
358 indicate further enrichment of this source in highly incompatible elements. In the Usun Apau
359 samples, increasing HFSE depletion with decreasing MgO (Figure 12a) suggests that this
360 signature may have been acquired in the crust owing to interaction with a HSFE depleted
361 contaminant (see section 6.3).

362 Macpherson et al. (2010) attributed the source of the SSA lavas to enrichment in the
363 convecting mantle available over a wide region, from the Sulu Arc to Hainan Island (Figure 1),
364 and proposed that the same mantle exists under central Borneo. We confirm this prediction is
365 true at least as far southwest as Linau Balui. The Usun Apau basalts are more enriched in the
366 most incompatible elements than the SSA lavas, suggesting that there may be subtle variations
367 in the composition of this source. Alternatively, the Usun Apau and Linau Balui basalts may
368 have originated from the same source through slightly smaller degrees of partial melting than
369 experienced at the SSA. This would be consistent with the greater lithospheric thickness
370 expected in southern Sarawak, compared to SSA, where Miocene subduction would have
371 thinned the overriding plate, onto which the latter were ultimately erupted.

372 *6.3 Differentiation: Mixing and Assimilation:* As established in the previous section, the
373 mafic lavas are probably related to a mantle component sampled by small degrees of partial

374 melting. As isotopic fractionation should not occur during fractional crystallization, the range of
375 the isotope ratios in the Usun Apau and Linau Balui volcanics provides unambiguous evidence
376 that mixing of one or more components contributed to their evolution. Strong inter-isotope
377 correlations indicate binary mixing. The fact that the Usun Apau and Linau Balui data plot in the
378 same arrays as the SSA (Figure 11) is strong evidence that the magmas from these regions
379 experienced similar evolutionary pathways with respect to source region and crustal assimilation.

380 In an attempt to constrain the origin of contamination in the SSA, Macpherson et al. (2010)
381 employed assimilation with fractional crystallization (AFC) modeling (De Paolo, 1981). The
382 SSA lavas are all basaltic or basaltic andesites, which restricts the amount of differentiation that
383 can be accommodated in such models. Hence, viable contaminants require large isotopic
384 differences from the uncontaminated melt. In practice, this meant a contaminant with very low
385 $^{143}\text{Nd}/^{144}\text{Nd}$ and, therefore, of great age, such as the Archean age granite Macpherson et al.
386 (2010) used to match the trends observed in the SSA. The situation is different for Usun Apau.
387 Because the volcanic rocks there also include more evolved dacites, a greater amount of
388 differentiation can be accommodated in AFC models which, in turn, decreases the amount of
389 isotopic leverage required of the contaminant. Therefore, it is more difficult to constrain the
390 isotopic composition of the contaminant or other parameters for the model e.g. bulk distribution
391 coefficients or the extent of assimilation.

392 We used Linau Balui basalt LB64 as a possible uncontaminated composition to test
393 possible AFC Models (Figure 14). LBA64 is considered suitable because, along with its lower
394 silica and magnesium contents, it has the highest $^{143}\text{Nd}/^{144}\text{Nd}$ and lowest $^{87}\text{Sr}/^{86}\text{Sr}$ in the area,
395 with values that lie within the field of South China Sea basalts (Figure 11a). Because little is
396 known about the composition of potential crustal contaminants in this part of Borneo, data were

397 compiled from a number of regional granitic belts that might offer approximate bulk crust
398 compositions. Since each of these display a spread in isotopic compositions, samples that
399 produced AFC models with the lowest $^{143}\text{Nd}/^{144}\text{Nd}$ at low $^{87}\text{Sr}/^{86}\text{Sr}$ were used because these, like
400 the Southern Sulu Arc (Macpherson et al. 2010), provide the best fit to the Linau Balui – Usun
401 Apau array. The one exception to this was for Triassic batholiths from the Malayan peninsula,
402 for which two compositions were used which span the range of Nd isotopic ratios. Ratios of
403 assimilation to crystallization (r) were varied between 0.15 and 0.3 but this has a negligible
404 impact upon the conclusions reached by this modeling (Figure 14).

405 Proterozoic metamorphic rocks of the Kontum massif in Vietnam and Mesozoic crust
406 similar to that of the South China margin, represented here by granitic rocks from Hong Kong
407 and the Dangerous Grounds attenuated crust, would be unsuitable contaminants as even their
408 lowest Nd isotopic values are too high for the required Sr signature (Figure 14b). Archean rocks,
409 which Macpherson et al. (2010) postulated to lie beneath the Southern Sulu Arc, can reproduce
410 the Linau Balui – Usun Apau array well (Figure 14a). An alternative contaminant, however, is
411 provided by the Malay Triassic batholiths. Less than 50% crystallization of the Linau Balui
412 basalt composition is required to generate the range of isotopic compositions in Usun Apau
413 dacites if melts resembling these granites were assimilated. The combination of a modest amount
414 of differentiation with modest values for r but of a silicic component could elevate SiO_2 contents
415 into the dacites range (Fig. 14a). The Malay Triassic batholiths, which had protoliths of mid-
416 Proterozoic crust (Liew and McCulloch, 1985), are associated with a world-class belt of tin
417 mineralization. We highlight the tin-bearing granites at Long Laai, 250 km east of Usun Apau
418 (Bambang and Le Bel, 1987; see Figure 3), as an intriguing occurrence indicating that similar
419 crust may underlie parts of the Luconia block.

420 6.4 *Luconia's Relationship to Other Crustal Blocks*: Regardless of the choice of protolith,
421 the isotopic data support the interpretation that differentiation of the Usun Apau, Linau Balui,
422 and South Sulu Arc magmas included assimilation of relatively old continental crust.
423 Macpherson et al. (2010) suggested that the Sulu Arc, the South China Sea region and its
424 extended margins are underlain by a common OIB-like mantle source with Dupal-like
425 characteristics (Tu et al. 1992), and that in some cases, depending on the ease of ascent through
426 the overlying crust, the isotopic signature of that source is significantly altered by interaction
427 with Precambrian continental crust. The OIB-like character of the Usun Apau and Linau-Balui
428 basalts (Figure 9) coupled with the trace element and isotopic signatures of the regional data set
429 (Figures 11 and 13) strongly suggests that similar lithosphere extends beyond the Tinjar Line and
430 underlies the Luconia block. The Linhaisai minettes in Kalimantan, interpreted as derived from
431 subcontinental lithosphere (Bergman et al. 1988), and tin-bearing granites at Long Laai having a
432 $^{87}\text{Sr}/^{86}\text{Sr}$ ratio of 0.7048 (Hutchison, 2010) further extends the potential geographic extent of this
433 continental basement (Figure 3). Thus, although the tectonic models generally treat the Borneo
434 region as comprised of multiple lithospheric blocks, it appears likely that the Greater Dangerous
435 Grounds, including the Luconia block and the Palawan micro-continent, represent lithospheric
436 fragments that share a distant Southeast Asian ancestry.

437 6.5 *Causes of Volcanism*: Intra-plate Plio-Pleistocene volcanic activity in the greater
438 South China Sea region poses an interesting question. How can such regional activity be
439 represented by widely scattered relatively small volumes of magma erupted in abrupt short-lived
440 pulses that appear to ultimately share a similar mantle source? We do not have a clear answer to
441 this question, but make some observations that point to several possibilities. Hainan Island is
442 underlain by a deep mantle plume that may represent melting of an EM2 mantle source (Zou and

443 Fan, 2010), whereas the Scarborough Seamounts appear to be related to paleo-transform faults of
444 the South China Sea spreading system. Borneo's interior volcanic tablelands, including the Usun
445 Apau and Linau Balui plateaus, are largely restricted to the region SW of the Tinjar Line (Figure
446 3), which is consistent with tectonic model that treat Luconia as a discrete lithospheric block.
447 With the exception of the Usun Apau calderas, which lie along the projection of faults that mark
448 the edge of Dulit plateau (Figure 2), the Tinjar Line does not appear to directly control the locus
449 of the volcanic activity. The varied settings for Pliocene volcanism point towards a deep seated
450 mechanism. Recent studies of shear wave velocity anisotropy in the region's upper mantle and
451 lower crust show that there are distinct areas with strong lateral gradients that persist vertically
452 for more than 200 km (Wu et al. 2005). Whilst these steep-sided lateral velocity gradients could
453 reflect temperature differences, we consider differences in volatile content related to dehydration
454 of an old deeply subducted slab to be a plausible complicating factor that is consistent with the
455 trace element geochemistry of the Usun Apau and Linau Balui volcanics. Regardless of their
456 ultimate origin, once primary melts are generated regional differences in lithospheric thickness,
457 as well as deeply rooted faults, related the region's protracted and complex tectonic history
458 influence further differentiation by controlling routes and rates of ascent.

459 7.0 CONCLUSIONS

- 460 • ^{39}Ar - ^{40}Ar age determinations show that two distinct pulses of volcanism are represented.
461 The Usun Apau dacites erupted at *ca.* 4.0 Ma; the Linau Balui and Usun Apau basalts
462 erupted at *ca.* 2.0 Ma.
- 463 • The Usun Apau and Linau Balui volcanic suites are the product of small percentage melting
464 of an LILE-enriched, OIB-like, garnet-bearing mantle possibly modified by fluids related to
465 much older subduction.

- 466 • Volcanic rocks from the Usun Apau and Linau Balui plateaus have isotopic signatures
467 indicating assimilation of relatively old continental crust.
- 468 • AFC modeling shows the Usun Apau dacites could be the product of fractional
469 crystallization coupled with assimilation of continental crust similar to the tin-bearing
470 Triassic Malay granites.
- 471 • The Tinjar Line does not appear to have played a direct role in magma genesis, but may
472 have localized emplacement by providing a route of ascent for the dacites.
- 473 • The Linau Balui and Usun Apau volcanics share radiogenic isotopic similarities not only
474 with the Southern Sulu Arc basalts, but also with other Pliocene basalts in the greater SCS
475 region. Thus, Luconia, the Dangerous Grounds, and the Palawan microplate appear to
476 represent crustal fragments that may ultimately share a Southeast Asian ancestry.

477 ACKNOWLEDGEMENTS

478 Morrison Ngau arranged most of the logistics and guided the expedition to Silio Falls of the
479 Usun Apau plateau. Without his help, good cheer, and perseverance that expedition would not
480 have achieved its objectives. We gratefully thank Morrison for all his hard work. Barry Weaver
481 of the University of Oklahoma was kind enough to review an early version of this paper. His
482 comments helped with improvements to several figures. Criticisms from an anonymous
483 reviewer helped to sharpen our discussion. Steve Bergman is acknowledged for his constructive
484 review that highlighted the importance of the Linhaisai minettes. Lastly, Robert Hall is thanked
485 for his encouragement and comments which helped to disambiguate several passages in the final
486 submission.

487 REFERENCES

- 488 Bambang, S., Le Bel, L.M., 1987. Discovery of a new tin province, Long Laai area, east
489 Kalimantan, Indonesia. In: Hutchison, C.S. (Ed.), Tin and Tungsten Granites, Proceedings
490 IGCP Project 220 Meeting, Sept. 1986. Technical Bulletin, 6. SEATRAD.
- 491
- 492 Banda, R.M., Aji, E., 2012. The Geology and Mineral Resources of the Northern Usun Apau
493 Area, Sarawak, Malaysia. Minerals and Geoscience Department of Malaysia Map Report 21, pp.
494 1-135.
- 495 Bergman, S. C., Dun, D. P., Krol, L. G. 1988. Rock and mineral of the Linhaisai Minette, Central
496 Kalimantan, Indonesia, and the origin of Borneo Diamonds. *Canadian Mineralogist* 26, 23-
497 43. Bird, P.R., Quinton, M.N., Bee, M.N., Bristow, J., 1993. Mindoro: a rifted microcontinent in
498 collision with the Philippines volcanic arc; basin evolution and hydrocarbon potential. *Journal of*
499 *Southeast Asian Earth Sciences* 8, 449-468.
- 500 Burton-Johnson, A., Macpherson, C. J., 2012. Mt. Kinabalu multi-phased post-collisional I-Type
501 granite. Abstract American Geophysical Union Annual Meeting.
- 502 Campbell, C.J., 1956. Geology of the Usun Apau area. *British Borneo Geological Survey Annual*
503 *Report*. pp. 86-120.
- 504 Camerlengo, A.L., Ambak, A.M., Saadon, M.N., 2000. Rainfall in Sarawak. *Pertanika Journal*
505 *of Science and Technology* 8, 125-135.
- 506 Chiang, K.K., 2002. Geochemistry of the Cenozoic igneous rocks of Borneo and tectonic
507 implications. Unpublished PhD thesis. Royal Holloway University of London, pp. 364.

508 Clift, P., Lee, G.H., Nguyen, A.D., Barckhausen, U., Long, H., Zhen, S., 2008. Seismic
509 reflection evidence for a Dangerous Grounds miniplate: No extrusion origin for the South China
510 Sea. *Tectonics* 27, 1-16.

511 Cottam, M., Hall, R., Sperber, C., Armstrong, R., 2010. Pulsed emplacement of layered granite:
512 new high-precision age data from Mount Kinabalu, North Borneo. *Journal of the Geological*
513 *Society of London* 176, 49-60.

514 Cullen, A.B., 2010. Transverse segmentation of the Baram-Balabac Basin, Northwest Borneo:
515 refining the model of Borneo's tectonic evolution. *Petroleum Geoscience* 16, 3–29.

516 Daly, M. C., Cooper, M. A., Wilson, I., Smith, D. G., Hooper, B. G., 1991. Cenozoic plate
517 tectonics and basin evolution in Indonesia. *Marine and Petroleum Geology* 8, 2-21.

518 Darbyshire, D. P. F., R. J. Sewell, 1997. "Nd and Sr isotope geochemistry of plutonic rocks from
519 Hong Kong: implications for granite petrogenesis, regional structure and crustal evolution."
520 *Chemical Geology* 143, 81-93.

521

522 DePaolo, D. J., 1981. Trace element and isotopic effects of combined wallrock assimilation and
523 fractional crystallization. *Earth and Planetary Science Letters* 53, 189-202.

524

525 Defant, M.J., Drummond, M.S., 1990. Derivation of some modern arc magmas by melting of
526 young subducted lithosphere. *Nature* 347, 662–665.

527 Elliott, T., 2003. Tracers of the slab. *Geophysical Monograph* 238, 23–45.

528

529 Green, D.H., Falloon, T.J., 2005. Primary magmas at mid-ocean ridges, “hotspots,” and other
530 intraplate settings: Constraints on mantle potential temperature. Geological Society of America
531 Special Paper 338, pp.32.

532 Hall, R., 1997. Cenozoic plate reconstructions of SE Asia. In: Hall, R., Blundell, D.J. (Eds.),
533 Tectonic Evolution of Southeast Asia, Geological Society of London Special Publication 106,
534 153-184.

535 Hall, R., 2002. Cenozoic geological and plate tectonic evolution of SE Asia and the SW Pacific:
536 computer-based reconstructions, model and animations. Journal of Asian Earth Sciences 20, 353-
537 431.

538 Hall, R., Nichols, G.J., 2002. Cenozoic sedimentation and tectonics in Borneo: climatic
539 influences on orogenesis. In: Jones, S.J., Frostick, L., (Eds), Sediment Flux in Basins, Causes,
540 Controls, and Consequences, Geological Society of London Special Publication 191, 5-22.

541 Hall, R., 2009. The Eurasian SE Asian margin as a modern example of an accretionary orogeny.
542 In: Cawood, P.A. and Kroner, A., (Eds.), Earth Accretionary Systems in Space and Time,
543 Geological Society of London, Special Publication 318, 351–372.

544 Hall, R., Clements, B., Smyth, H.R., 2009. Sundaland basement character, structure and plate
545 tectonic development. In: Proceedings Indonesian Petroleum Association, 33rd Annual
546 Convention, IPA09-G-134,1–27.

547 Hamilton, W., 1979. Tectonics of the Indonesian region. United States Geological Survey
548 Professional Paper 1078, pp. 345.

549 Handley, H.K., Macpherson, C.G., Davidson, J.P., Berlo, K., Lowry, D., 2007. Constraining
550 fluid and sediment contributions to subduction-related magmatism in Indonesia: Ijen
551 Volcanic Complex. *Journal of Petrology* 48, 1155–1183.
552

553 Hart, S.R., 1984. A large-scale isotope anomaly in the Southern Hemisphere mantle.
554 *Nature* 309, 753–757.
555

556 Hazenbroek, H.P., Morshidi, A.K., 2001. National Parks of Sarawak. *Natural History*
557 *Publications (Borneo)*, Kota Kinabalu, pp. 502.
558

559 Holloway, N. H., 1982, North Palawan Block, Philippines – Its Relation to Asian Mainland and
560 Role in the Evolution of South China Sea. *American Association of Petroleum Geologists*,
561 *Bulletin* 66, 1355-1383.
562

563 Hutchison, C.S. 1996. The 'Rajang Accretionary Prism' and 'Lupar Line' Problem of Borneo. In:
564 Hall, R., Blundell, D.J. (Eds.), *Tectonic Evolution of Southeast Asia*, Geological Society of
565 London Special Publication 106, 247-261.

566 Hutchison, C.S., 2005. *Geology of North-West Borneo*: Elsevier, Amsterdam, Netherlands, pp.
567 421.

568 Hutchison, C.S., 2010. Oroclines and paleomagnetism in Borneo and South-East Asia.
569 *Tectonophysics* 496, 53–67.

570 Hutchison, C.S., Bergman, S.C., Swauger, D., Graves, J.E., 2000. A Miocene collisional belt in
571 north Borneo, uplift mechanism and isostatic adjustment quantified by thermochronology.
572 *Journal of the Geological Society of London* 157, 783–793.

573

574 Jacobsen, S. B., G. Wasserburg (1978). "Interpretation of Nd, Sr and Pb isotope data from
575 Archean migmatites in Lofoten-Vesterålen, Norway." *Earth and Planetary Science Letters* 41(3):
576 245-253.

577

578 Johnson, D.M., Hooper P.R., Conrey, R.M., 1999. XRF Analysis of Rocks and Minerals for
579 Major and Trace Elements on a Single Low Dilution Li-tetraborate Fused Bead. *Advances in X-
580 Ray Analysis* 41, 843-867.

581 Kirk, H.J., 1957. The geology and mineral resources of the upper Rajang and adjacent areas.
582 *Geological Survey Department British Territories in Borneo, Memoir 8*, pp. 181.

583 Kirk, H.J., 1968. The Igneous Rocks of Sarawak and Sabah. *Geological Survey of Borneo
584 Region, Malaysia, Bulletin 5*, pp. 210.

585 Kudrass, H. R., Wiedicke, M., Cepek, P., Kreuzer, H., Muller, P., 1986. Mesozoic and Cainozoic
586 rocks dredged from the South China Sea (Reed Bank area) and Sulu Sea and their significance
587 for the plate-tectonic reconstructions. *Marine and Petroleum Geology* 3, 19–30.

588 Lan, C.Y., Chung, S.L., Lo, C.H., Lee, T.Y., Wang, P.L., Li, H., Toan, D.V., 2001. First
589 evidence for Archean continental crust in northern Vietnam and its implications for crustal and
590 tectonic evolution in Southeast Asia. *Geology* 29, 219–222.

591 Lan, C.Y., S.L. Chung, S. L., Long, T. C., Lo, C. H., Lee, T. Y., Mertzman, S. A., Shen, J. J.,
592 2003. Geochemical Sr–Nd isotopic constraints from the Kontum Massif, central Vietnam, on the
593 crustal evolution of the Indochina block. *Precambrian Research* 122, 7–27.

594 Le Bas, M. J., Streckeisen, A.L., 1991. The IUGS systematic of igneous rocks. *Journal of the*
595 *Geological Society London* 148, 825-833.

596 Liew, T. C., McCulloch, M. T., 1985. Genesis of granitoid batholiths of Peninsular Malaysia and
597 implications for models of crustal evolution: Evidence from a Nd-Sr isotopic and U-Pb zircon
598 study. *Geochimica et Cosmochimica Acta* 49, 587-600.

599 Longley, I. M., 1997. The tectonostratigraphic evolution of SE Asia. In: Murphy, R. W. (Ed.),
600 *Petroleum Geology of Southeast Asia*, Geological Society of London Special Publication 126,
601 311-339.

602 Macpherson, C.G., Chaing, K., Hall, R., Nowell, G. M., Castillo, P. R., Thirlwall, M. F., 2010.
603 Plio-Pleistocene intra-plate magmatism from the southern Sulu Arc, Semporna peninsula, Sabah,
604 Borneo: Implications for high-Nb basalt in subduction zones. *Journal of Volcanology and*
605 *Geothermal Research* 190, 25-38.

606 Macpherson, C.G., Dreher, S.T., Thirlwall, M.F., 2006. Adakites without slab melting: high
607 pressure processing of basaltic island arc magma, Mindanao, Philippines. *Earth and Planetary*
608 *Science Letters* 243, 581–593.

609

610 McLeod, C. I., 2012. An investigation of crustal contamination through petrology and
611 geochemistry. PhD Thesis, Durham University, UK

612 Metcalfe, I., 2010. Tectonic framework and Phanerozoic evolution of Sundaland. *Gondwana*
613 *Research* 19, 3–21.

614 Milsom, J., Holt, R., 2001. Discussion of a Miocene collisional belt in north Borneo, uplift
615 mechanism and isostatic adjustment quantified by thermochronology. *Journal of the Geological*
616 *Society London* 158, 396-400.

617 Morley, C.K., 2002. A tectonic model for the Tertiary evolution of strike-slip faults and rift
618 basins in SE Asia. *Tectonophysics* 347, 189-215

619 Moss, S. J., 1998. Embaluh Group turbidites in Kalimantan: evolution of a remnant ocean basin
620 in Borneo during the late Cretaceous to Paleogene. *Journal of the Geological Society of London*
621 155, 509-524.

622 Moss, S.J., Carter, A., Bakers, S., Herford, A.J., 1998. A Late Oligocene tectono-volcanic event
623 in East Kalimantan and the implications for tectonics and sedimentation in Borneo. *Journal of*
624 *the Geological Society of London* 155, 177–192.

625 Pieters, P. E., Supriatna, S., 1990. Preliminary geological map of west, central, and east
626 Kalimantan area. Indonesia Geological Development and Research Centre.

627

628 Prouteau, G., Maury, R.C., Sajona, F.G., Pubellier, M., Cotten, J. & Bellon, H., 2001. Le
629 magmatisme post-collisionnel du Nord-Ouest de Bornéo, produit de la fusion d'un fragment de
630 croûte océanique ancré dans le manteau supérieur. *Bulletin de la Société Géologique de France*
631 172, 319–332.

632 Rapp, R.P., Shimizu, N., Norman, M.D., Applegate, G.S., 1999. Reaction between slab-derived
633 melts and peridotite in the mantle wedge: experimental constraints at 3.8 GPa. *Chemical*
634 *Geology* 160, 335-356.

635 Renne, P.R., Swisher, C.C., Deino, A.L., Karner, D.B., Owens, T.L., DePaolo, D.J., 1998.
636 Intercalibration of standards, absolute ages and uncertainties in $^{40}\text{Ar}/^{39}\text{Ar}$ dating. *Chemical*
637 *Geology* 145, 117-152.

638

639 Satyana, A. H., Nugroho, D., Imanhardjo S., 1999. Tectonic controls on the hydrocarbon habitats
640 of the Barito, Kutei, and Tarakan Basins, Eastern Kalimantan, Indonesia: major dissimilarities in
641 adjoining basins. *Journal of Asian Earth Sciences* 17, 99-122. Soeria-Atmadja, R., Noeradi, D.,
642 Pridai, P., 1999. Cenozoic magmatism in Kalimantan and its related geodynamic evolution.
643 *Journal of Asian Earth Science* 17, 25-45.

644 Staudacher, T.H., Jessberger, E.K., Dorflinger, D., Kiko, J., 1978. A refined ultrahigh-vacuum
645 furnace for rare gas analysis. *Journal Physics of Earth Science Instrumentation* 11, 781-784.

646

647 Stern, R. J., 2002. Subduction Zones. *Reviews in Geophysics* 40, 1-42.

648

649 Sun, S.S., McDonough, W.F., 1989. Chemical and isotopic systematics of oceanic basalts:
650 implications for mantle composition and processes. In: Saunders, A.D., Norry, M.J. (Eds.),
651 *Magmatism in the Ocean Basins: Geological Society of London Special Publication* 42, 313–
652 345.

653 Taib, N.I., 2010. K-rich basalt in the Bukit Mersing area, Third Division, Sarawak. *Geological*
654 *Society Malaysia Bulletin* 52, 67-73.

655

656 Taib, N.I., 2012. Bimodal Cenozoic Volcanism in Central Sarawak: Hot Spots or Extension?
657 Proceedings of GEOSEA2012, 60.

658

659 Tate, R.B., 2001. Geological Map of Borneo Island. CD-ROM. Geological Society of Malaysia.

660

661 Tu, K., Flower, M.F.J., Carlson, R.W., Xie, G.H., Chen, C.Y., Zhang, M., 1992. Magmatism in
662 the South China Basin, 1. Isotopic and trace element evidence for an endogenous Dupal mantle
663 component. *Chemical Geology* 97, 47–63.

664

665 Van Bemmelen, R.W., 1949. The Geology of Indonesia, 1A, General Geology of Indonesia and
666 Adjacent Archipelagoes. 732 pp., Government Printing Office, The Hague

667

668 van Hattum, M., Hall, R., Pickard, A., Nichols, G., 2006. Southeast Asian sediments not from
669 Asia: Provenance and geochronology of north Borneo sandstones. *Geology* 34, 589–592.

670

671 van Leeuwen, T.M., Leach, T., Hawke, A.A., Hawke, M.M., 1990. The Kelian disseminated
672 gold deposit, East Kalimantan, Indonesia: An example of a deeply eroded epithermal system.
673 In: J.W. Hedenquist, N.C. White and G. Siddeley (Editors), *Epithermal Gold Deposits of the*
674 *Circum-Pacific: Geology, Geochemistry, Origin and Exploration*, *Journal Geochemical*
675 *Exploration* 35, 1-61.

676

677 Wooden, J., P., Mueller, J. P., 1988. Pb, Sr, and Nd isotopic compositions of a suite of Late
678 Archean, igneous rocks, eastern Beartooth Mountains: implications for crust-mantle evolution.

679 Earth and Planetary Science Letters 87, 59-72. Wu, H.H., Tsai, Y., Lee, T.Y., Lo, C.H., Hseih,
680 C.H., Toan, D., 2005. 3-D shear wave velocity structure of the crust and upper mantle in South
681 China Sea and its surrounding regions by surface wave dispersion analysis. Marine Geophysical
682 Research 25, 5–27

683 Wendt, I., Carl, C., 1991. The statistical distribution of the mean squared weighted deviation.
684 Chemical Geology 86, 275-285.

685

686 Yan, Q. S., X. F. Shi, J. H. Liu, K. S. Wang, K. S., Bu, W. R., (2010). "Petrology and
687 geochemistry of Mesozoic granitic rocks from the Nansha micro-block, the South China Sea:
688 Constraints on the basement nature. Journal of Asian Earth Sciences 37, 130-139.

689 Yan, Q., Shi, X., Li, N., 2011. Oxygen and lead isotope characteristics of granitic rocks from the
690 Nansha block (South China Sea): Implications for their petrogenesis and tectonic affinity. Island
691 Arc 20, 150-159.

692

693 Zou, H., Fan, Q., 2010. U–Th isotopes in Hainan basalts: Implications for sub-asthenospheric
694 origin of EM2 mantle end-member and the dynamics of melting beneath Hainan Island. Lithos
695 116, 145-152. Yan, Q., Shi, X., Lui, J, Wang, K. Bu, W., 2010. Petrology and geochemistry of
696 Mesozoic granitic rocks from the Nansha micro-block, the South China Sea: Constraints on the
697 basement nature. Journal of Asian Earth Sciences 34, 30-39.

698

699 Yumul, G.P., Dimalanta, C.B., Marquez E. J., Queaño K. L., 2009. Onland signatures of the
700 Palawan microcontinental block and Philippine mobile belt collision and crustal growth process:
701 a review. Journal of Asian Earth Sciences 34, 610-623.

702

703 Yogodzinski, G. M., Kay, R. W., Volynets, O. N Koloskov, A.V., Kay, S.M., 1995. Magnesian
704 andesite in the western Aleutian Komandorsky region: implications for slab melting and
705 processes in the mantle wedge. Geological Society of America Bulletin 107, 505-519.

706 FIGURE CAPTIONS

707 Figure 1 1a) Maps showing location of study area in relation principal tectonic component of the
708 Borneo region. Abbreviation: BD- Baram Delta, BL-Balabac Line, CS- Celebes Sea, DGs-
709 Dangerous Grounds, HI- Hainan Island, KAL- Kalimantan, KM- Kontum Massif, KU- Kuching,
710 LB- Linau-Balui plateau, LUB- Luconica Block, LL-Lupar Line, MK- Mount Kinabalu, MT-
711 Manila trench, NWBT- Northwest Borneo Trough with limit of deepwater fold-thrust belt in
712 dashed line with open triangles, RB-Reed Bank, RJD- Rajang Delta, SCS- South China Sea with
713 oceanic crust outline in gray dashed line and 200m isobaths in dotted line, SA- Sulu Arc, SAB-
714 Sabah, SM- Schwaner Mountains, SS-Sulu Sea, SSA- Southern Sulu Arc SWB- Southwest
715 Borneo Block, SWK- Sarawak, UP- Usun Apau, WBL- West Baram Line; strongly deformed
716 Paleogene flysch of Borneo highlands shown as gray shaded areas. Question marks (?) highlight
717 areas of uncertain relationships. 1b- Schematic illustration of NW Borneo region's crustal blocks
718 and tectonic setting circa 35 Ma: abbreviations as before; NBPB- North Borneo Palawan Blocks,
719 SPB- South Palawan Block. Lines with solid triangles denote upper plate of suture zones.
720 (Longley, 1996; Hall, 1997; Morley, 2002, Hall et al. 2009)

721 Figure 2 Geological features of the Usun Apau area: Topographic relief map as background,
722 volcanic plateau in light gray with sample locations posted, fold axes of strongly deformed
723 Paleogene deepwater clastic rocks in dashed black lines. Dashed grey lines and (f) mark faults
724 that bound the NE edge of the Dulit plateau approximately 20km northwest of the Usun Apau
725 plateau. Inset is a Google Earth image of eastern side of plateau.

726 Figure 3 Map showing distribution and age of Cenozoic igneous rocks in relation to tectonic
727 elements discussed in text. Abbreviations as before and those shown in legend. Open triangles

728 show the different ages of position of subduction tip line in the different tectonic reconstructions
729 of Hall (2002 and 2009).

730 Figure 4 Outcrop photo at Silio Falls (ca. 200m) shows contact between crudely jointed lava
731 flows (UP-D) and overlying welded tuffs (UP-WT).

732 Figure 5 Photomicrographs of Usun Apau volcanic rocks. 5a) polarized light, welded tuff with
733 embayed quartz xenocryst(Q) in glassy ground mass with exquisite flow patterns with euhedral
734 hypersthene phenocryst (H); 5b) cross-polarized light, welded tuff, quartz xenocryst with fine
735 rutile inclusions (R); 5c) polarized light, oscillatory-zoned Carlsbad twinned plagioclase
736 phenocryst; 5d) plain light, trachytic plagioclase laths in fine-grained groundmass

737 Figure 6 Plot of Ar-Ar age as a function of % ³⁹Ar released during stepwise heating for 3 mineral
738 separate samples.

739 Figure 7 Total alkali silica classification (Le Bas and Streikeisen, 1982) of samples from Linau
740 Balui and Usun Apau plateaus plotted with data from the Sintang suite near Kuching (Prouteau
741 et al. 2001), Linhaisai minettes (Bergman et al. 1987), Southern Sulu Arc (Macpherson et al.
742 2010), and Bukit Mersing (Taib, 2010).

743 Figure 8 Plot of major and trace element data for the Usun Apau and Linau-Balui volcanics; TN,
744 Tinjar; BM Bukit Mabun. 8a) Selected major elements versus SiO₂. 8b) Selected trace elements
745 versus wt. % SiO₂

746 Figure 9 Normalized Rock/ N-MORB plot for selected trace elements comparing Usun Apau
747 and Linau Balui; N-MORB and OIB from Sun and McDonough (1989); Island Arc Basalt- IAB
748 (Elliott, 2003).

749 Figure 10 Plots of 12a) $^{87}\text{Sr}/^{86}\text{Sr}$ vs. SiO_2 and 12b) $^{143}\text{Nd}/^{144}\text{Nd}$ vs. SiO_2 for the Usun Apau and
750 Linau Balui volcanics

751

752 Figure 11 $^{87}\text{Sr}/^{86}\text{Sr}$, $^{143}\text{Nd}/^{144}\text{Nd}$, $^{206}\text{Pb}/^{204}\text{Pb}$, $^{207}\text{Pb}/^{204}\text{Pb}$, and $^{208}\text{Pb}/^{204}\text{Pb}$ isotopic data from Usun
753 Apau, Linau Balui, and Tinar Line plotted with data from other Cenozoic igneous rocks from the
754 greater SCS region: DG- Dangerous Grounds (Yan et al. 2010; Yan et al. 2010), Bukit Mersing
755 Taib (2012), shaded polygons for the Northern & Central Sulu Arc and Hainan Island & South
756 China Sea (Macpherson et al. 2010 and references therein); NHRL, Northern Hemisphere
757 Reference Line (Hart, 1984); I-MORB Indian Ocean MORB (GERM: <http://earthref.org/GERM>)

758

759 Figure 12 Trace element plots comparing Usun Apau (UP) and Linau Balui (LB) samples with
760 other igneous rocks from NW Borneo (Prouteau et al. 2001; Macpherson et al. 2010). 10a) Nb
761 vs. wt% MgO, 10b) Sr/Y vs. Y discrimination diagram (Defant and Drummond, 1990), 10c) ppm
762 Rb vs. wt % SiO_2 , 11d) K/Rb vs. wt % SiO_2

763 Figure 13 Averaged normalized Rock/ N-MORB plot for selected trace elements comparing the
764 Usun Apau and Linau Balui plateaus with areas previously discussed and referenced in figures
765 11 and 12.

766

767 Figure 14 Assimilation fractional crystallization models. $^{143}\text{Nd}/^{144}\text{Nd}$ versus $^{87}\text{Sr}/^{86}\text{Sr}$ for
768 volcanic rocks from Usun Apau (squares) and Linau Balui (circles). Lines represent assimilation
769 and fractional crystallization models (DePaolo, 1981) of (a) suitable, and (b) unsuitable
770 contaminants to generate the Usun Apau – Linau Balui array. Initial basalt is Linau Balui basalt

771 (LBA64; this work) $^{87}\text{Sr}/^{86}\text{Sr} = 0.704100$, $^{143}\text{Nd}/^{144}\text{Nd} = 0.512879$, Sr = 289 ppm, Nd = 13 ppm.
772 In all models, $D_{\text{Sr}} = 1.5$ and $D_{\text{Nd}} = 0.1$. Contaminant compositions are Triassic batholiths of the
773 East Coast of Peninsular Malaysia, samples 93 and 106 (Liew and McCulloch 1985); $^{87}\text{Sr}/^{86}\text{Sr} =$
774 0.706760 and 0.811870 , $^{143}\text{Nd}/^{144}\text{Nd} = 0.5116300$ and 0.511490 , Sr = 31 and 719 ppm, Nd = 28
775 and 35 ppm; Archean crust, Beartooth Mountains, USA (Wooden and Mueller 1988) $^{87}\text{Sr}/^{86}\text{Sr} =$
776 0.724600 , $^{143}\text{Nd}/^{144}\text{Nd} = 0.510250$, Sr = 400ppm, Nd = 43 ppm; Archean migmatite, Lofoten-
777 Verterålen, Norway (Jacobsen and Wasserburg 1978) $^{87}\text{Sr}/^{86}\text{Sr} = 0.708900$, $^{143}\text{Nd}/^{144}\text{Nd} =$
778 0.510410 , Sr = 573 ppm, Nd = 29ppm; Metamorphic rocks of the Kontum Massif, Vietnam
779 (Lan, Chung et al. 2003) $^{87}\text{Sr}/^{86}\text{Sr} = 0.706210$, $^{143}\text{Nd}/^{144}\text{Nd} = 0.512323$, Sr = 848ppm, Nd =
780 16ppm; Dangerous Grounds attenuated crust (Yan, Shi et al. 2010) $^{87}\text{Sr}/^{86}\text{Sr} = 0.711624$,
781 $^{143}\text{Nd}/^{144}\text{Nd} = 0.512030$, Sr = 470 ppm, Nd = 33 ppm. Granitic rocks from Hong Kong
782 (Darbyshire and Sewell 1997) $^{87}\text{Sr}/^{86}\text{Sr} = 0.711491$, $^{143}\text{Nd}/^{144}\text{Nd} = 0.512344$, Sr = 271 ppm, Nd
783 = 41 ppm. Two curves are shown for each contaminant representing different values for r ; the
784 ratio of mass assimilated to mass crystallized. Except for the Malay Batholiths the end members
785 are the same with $r = 0.15$ for the higher- $^{143}\text{Nd}/^{144}\text{Nd}$ model and $r = 0.3$ for the lower-
786 $^{143}\text{Nd}/^{144}\text{Nd}$ model. The Malay Batholith models are for different contaminants ($r = 0.3$ and 0.15 ,
787 respectively for the pairs of values listed above). Models run cover range of F ; fraction of liquid
788 remaining, from 1 – 0.1. F values are indicated on Malay Batholith models decreasing in 0.1
789 increments.

790

791

792 TABLE CAPTIONS

793 Table 1 Results of ^{39}Ar - ^{40}Ar Age Determinations

794 Table 2 Major and Trace Element Analyses: Major element oxides normalized to 100% on a
795 volatile-free basis.

796 Table 3 Radiogenic Isotope Analyses

797 **APPENDIX A: ANALYTICAL METHODS**

798 **Age Determinations:** Radiometric age determinations were analyzed by the $^{40}\text{Ar}/^{39}\text{Ar}$ method at
799 the Nevada Isotope Geochronology Laboratory (University of Nevada Las Vegas). Samples were
800 wrapped in Al foil and stacked in 6 mm inside diameter sealed fused silica tubes. Individual
801 packets averaged 3 mm thick and neutron fluence monitors (FC-2, Fish Canyon Tuff sanidine)
802 were placed every 5-10 mm along the tube. Synthetic K-glass and optical grade CaF_2 were
803 included in the irradiation packages to monitor neutron induced argon interferences from K and
804 Ca. Loaded tubes were packed in an Al container and irradiated at the U. S. Geological Survey
805 TRIGA Reactor, Denver, CO in the In-Core Irradiation Tube (ICIT) of the 1 MW TRIGA type
806 reactor. Correction factors for interfering neutron reactions on K and Ca were determined by
807 repeated analysis of K-glass and CaF_2 fragments. Measured $(^{40}\text{Ar}/^{39}\text{Ar})_{\text{K}}$ values were $1.48 (\pm$
808 $79.07\%) \times 10^{-2}$. Ca correction factors were $(^{36}\text{Ar}/^{37}\text{Ar})_{\text{Ca}} = 2.60 (\pm 3.15\%) \times 10^{-4}$ and
809 $(^{39}\text{Ar}/^{37}\text{Ar})_{\text{Ca}} = 6.70 (\pm 1.70\%) \times 10^{-4}$. J factors were determined by fusion of 4-8 individual
810 crystals of neutron fluence monitors which gave reproducibility's of 0.25% to 0.48% at each
811 standard position. Variation in neutron fluence along the 100 mm length of the irradiation tubes
812 was <4%. Matlab curve fit was used to determine J and uncertainty in J at each standard
813 position. No significant neutron fluence gradients were present within individual packets of
814 crystals as indicated by the excellent reproducibility of the single crystal fluence monitor fusions.

815 Irradiated FC-2 sanidine standards together with CaF₂ and K-glass fragments were placed
816 in a Cu sample tray in a high vacuum extraction line and were fused using a 20 W CO₂ laser.
817 Sample viewing during laser fusion was by a video camera system and positioning was via a
818 motorized sample stage. Samples analyzed by the furnace step heating method utilized a double
819 vacuum resistance furnace similar to the Staudacher et al. (1978) design. Reactive gases were
820 removed by three GP-50 SAES getters prior to being admitted to a MAP 215-50 mass
821 spectrometer by expansion. The relative volumes of the extraction line and mass spectrometer
822 allow 80% of the gas to be admitted to the mass spectrometer for laser fusion analyses and 76%
823 for furnace heating analyses. Peak intensities were measured using a Balzers electron multiplier
824 by peak hopping through 7 cycles; initial peak heights were determined by linear regression to
825 the time of gas admission. Mass spectrometer discrimination and sensitivity was monitored by
826 repeated analysis of atmospheric argon aliquots from an on-line pipette system. Measured
827 ⁴⁰Ar/³⁶Ar ratios were 283.23 ± 0.20% during this work, thus a discrimination correction of
828 1.0433 (4 AMU) was applied to measured isotope ratios. The sensitivity of the mass
829 spectrometer was ~6 x 10⁻¹⁷ mol mV⁻¹ with the multiplier operated at a gain of 36 over the
830 Faraday. Line blanks averaged 26.20 mV for mass 40 and 0.02 mV for mass 36 for laser fusion
831 analyses and 24.32 mV for mass 40 and 0.08 mV for mass 36 for furnace heating analyses.
832 Discrimination, sensitivity, and blanks were relatively constant over the period of data collection.
833 Computer automated operation of the sample stage, laser, extraction line and mass spectrometer
834 as well as final data reduction and age calculations were done using LabSPEC software written
835 by B. Idleman (Lehigh University). An age of 28.02 Ma (Renne et al. 1988) was used for the
836 Fish Canyon Tuff sanidine fluence monitor in calculating ages for samples.

837 For $^{40}\text{Ar}/^{39}\text{Ar}$ analyses a plateau segment consists of 3 or more contiguous gas fractions
838 having analytically indistinguishable ages (i.e. all plateau steps overlap in age at $\pm 2\sigma$ analytical
839 error) and comprising a significant portion of the total gas released (typically >50%). Total gas
840 (integrated) ages are calculated by weighting by the amount of ^{39}Ar released, whereas plateau
841 ages are weighted by the inverse of the variance. For each sample inverse isochron diagrams are
842 examined to check for the effects of excess argon. Reliable isochrons are based on the MSWD
843 criteria of Wendt and Carl (1991) and, as for plateaus, must comprise contiguous steps and a
844 significant fraction of the total gas released. All analytical data are reported at the confidence
845 level of 1σ (standard deviation). Furnace step heating analyses produce an apparent age
846 spectrum. The "apparent" derives from the fact that ages on an age spectrum plot are calculated
847 assuming that the non-radiogenic argon (trapped initial argon) is atmospheric in isotopic
848 composition ($^{40}\text{Ar}/^{36}\text{Ar} = 295.5$). Isochrons can verify (or rule out) excess argon, and isochron
849 ages are usually preferred if a statistically valid regression is obtained. If there is excess argon in
850 the sample ($^{40}\text{Ar}/^{36}\text{Ar} > 295.5$) then these apparent ages will be older than the actual age of the
851 sample. U-shaped age spectra are commonly associated with excess argon (the first few and
852 final few steps often have lower radiogenic yields, thus apparent ages calculated for these steps
853 are affected more by any excess argon present). When such a sample yields no reliable
854 isochron, the youngest measured age provides a maximum estimate for the age of the sample.
855 Plateau ages are simply a segment of the age spectrum which consists of 3 or more steps,
856 comprising >50% of the total gas released. An isochron age is the best estimate of the age of a
857 sample, even if a plateau age is obtained. $^{40}\text{Ar}/^{39}\text{Ar}$. Total gas ages are equivalent to K/Ar ages
858 determined by older analytical methods.

859 **Major and Trace Elements:** KL49, UA14, AN35, UA52, UP3, UP4, UP5, UP6, UP7, UP8 and
860 UP9 were analyzed for major elements by X-ray Fluorescence Spectroscopy (XRF) at the
861 Geoanalytical Lab at Washington State University, United States,, using the low-dilution fused
862 bead method described in Johnson et al. (1999). UA81, UA43, Tn96 and LBA64, LBA84 and
863 LBA98 were analyzed for major elements using a Pan-Analytical Axios Max WD-RXF at
864 University of Malaya, Malaysia, using 1:9 dilution fused beads with a lithium tetraborate flux
865 (Fluxana FX-X100). Powdered samples were heated at 950 degrees C to determine Loss on
866 Ignition values, after which they were mixed with flux in platinum crucibles and fused over a
867 propane-oxygen flame in a HD Elektronik Vulcan automatic fusion machine. After an automated
868 cycle of heating and agitation, the molten charge was poured onto heated platinum moulds to
869 produce 32mm buttons. Calibration used nine USGS rock standards prepared in the same way as
870 the samples. These samples were also analyzed for trace elements using a Thermo Scientific -
871 XSeries II ICP-MS at the *Vrije Universiteit*, Amsterdam

872 The UP samples trace elements were also measured by XRF; precision was determined by
873 triplicate analysis of separate glass beads prepared from sample of Galapagos basalt, run at the
874 same time as the Usun Apau samples. The relative standard deviation on the triplicate analyses is
875 <1% except for FeO_t(2.0%), K₂O (1.1%), and Na₂O (2.6%). Samples KL49, UA14, AN35,
876 UA52 were analyzed for trace elements, including rare earth elements, by Inductively Coupled
877 Plasma Mass Spectrometry (ICP-MS); methods and standards can be found at
878 <http://www.sees.wsu.edu/Geolab/note/icpms.html>.

879 **Radiogenic Isotopes:** UA81, UA43, Tn96, LBA64, LBA84, and LBA98 were analyzed for Pb,
880 Nd and Sr isotopes at the *Vrije Universiteit*, Amsterdam, using ultra-clean dissolution in teflon
881 beakers and ion-exchange resin columns. Sr isotopes were measured using TIMS (Finnigan

882 MAT 262) and Pb and Nd isotopes were measured using a Finnigan Neptune multi-collector
883 ICP-MS. BHVO-2 and BCR-2 were used as internal check standards for trace and isotope
884 analyses. The UP samples were analysed for Sr, Nd and Pb isotopes at Northern Centre for
885 Isotopic and Elemental Tracing, Durham University, United Kingdom. Isotope ratios in the
886 fractions for Sr, Nd and Pb were measured using the ThermoElectron Neptune PIMMS (Plasma
887 Ionisation Multi-collector Mass Spectrometer). Details of operating procedures and instrument
888 configuration are given in Mcleod (2012). Measured values for the NBS 987 Sr and J&M Nd
889 standards $\pm 2SD$ error obtained during the same runs as the UP samples were 0.710269 ± 0.000028
890 ($n=11$) and 0.511112 ± 0.000008 ($n=15$), respectively. The NBS 981 Pb standard gave ratios
891 averaging 16.94051 ± 0.000906 for $^{206}\text{Pb}/^{204}\text{Pb}$, 15.49800 ± 0.000754 for $^{207}\text{Pb}/^{204}\text{Pb}$ and
892 36.71744 ± 0.002327 for $^{208}\text{Pb}/^{204}\text{Pb}$

893

894

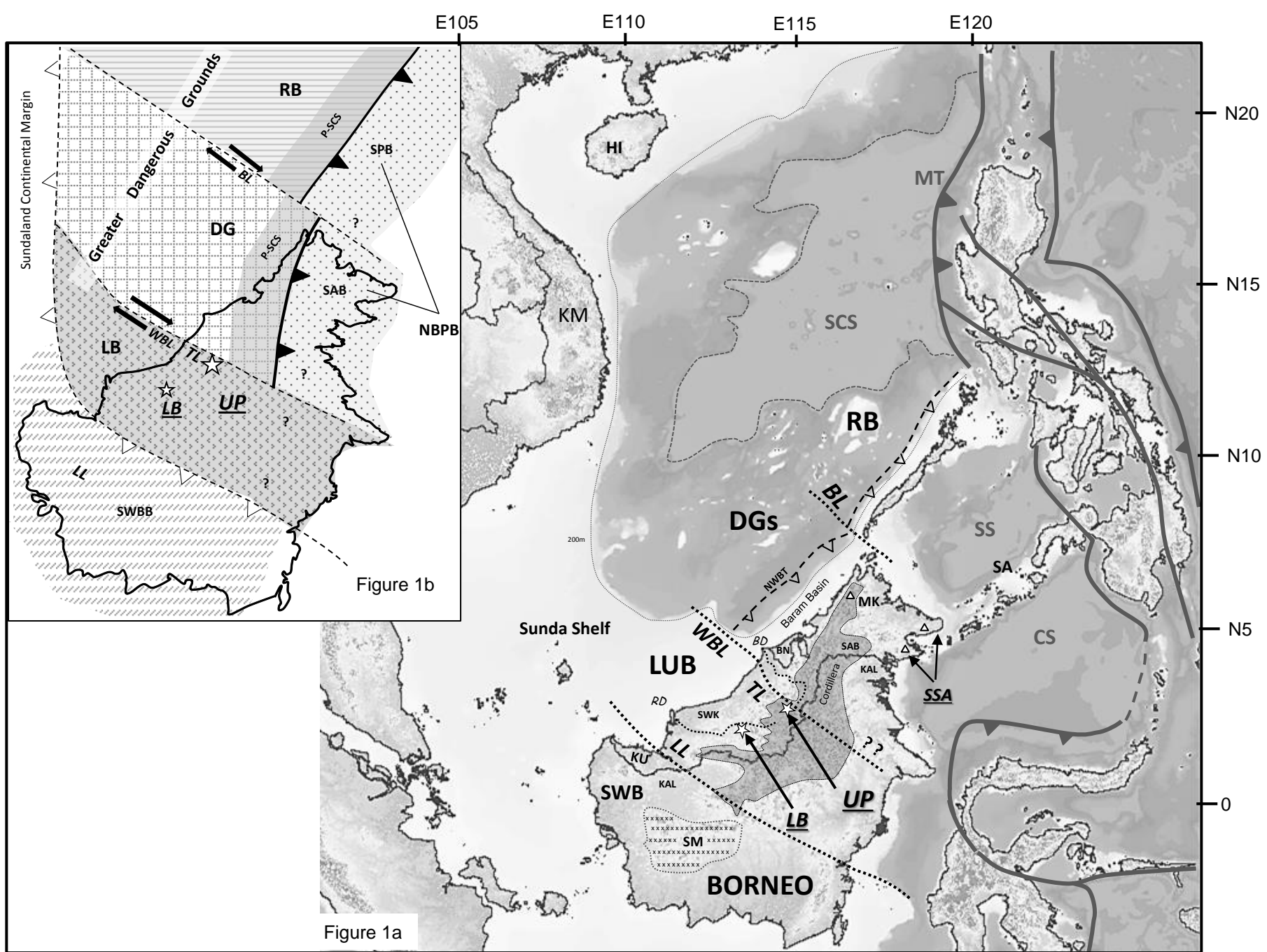


Figure 1

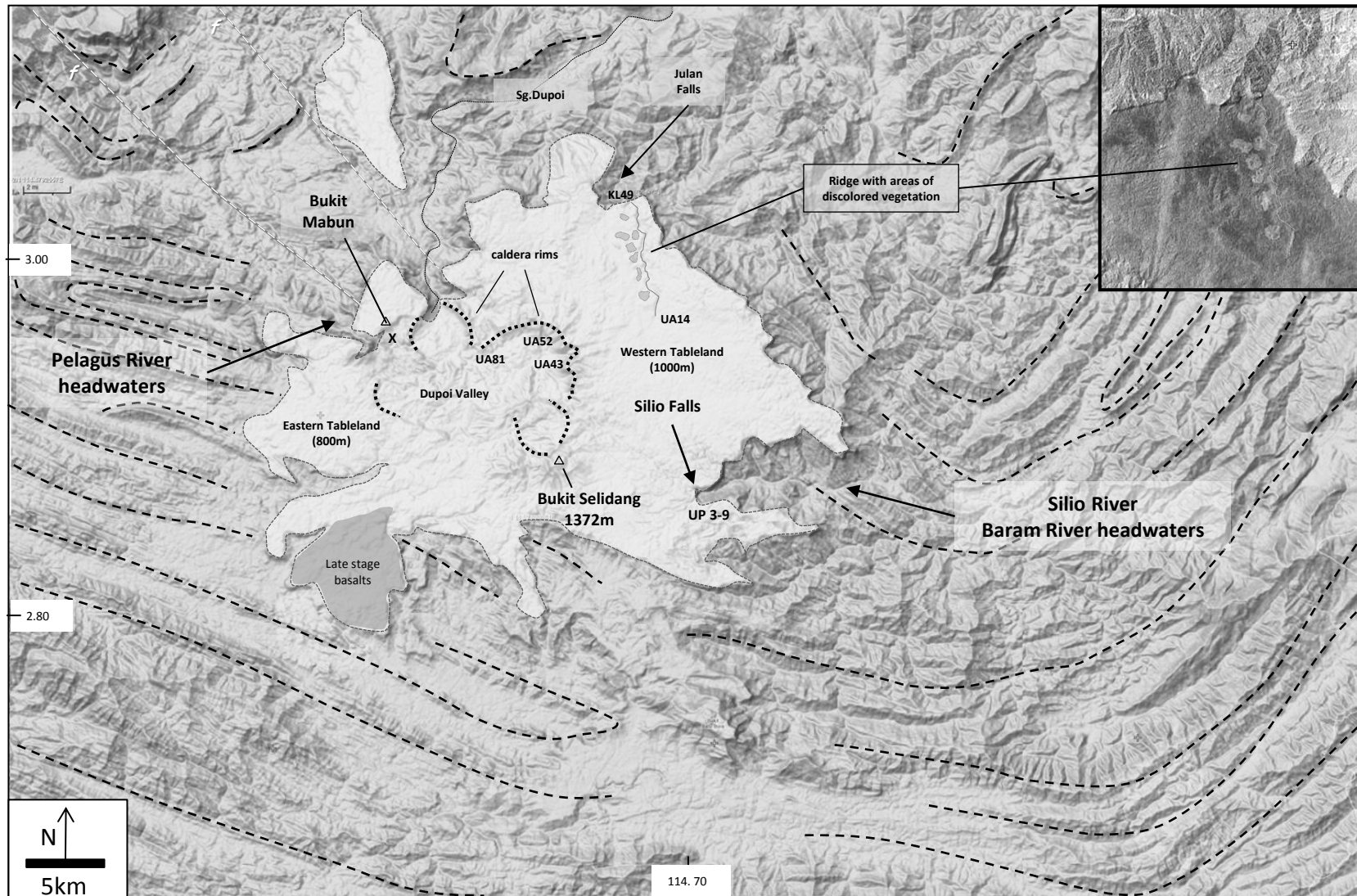


Figure 2

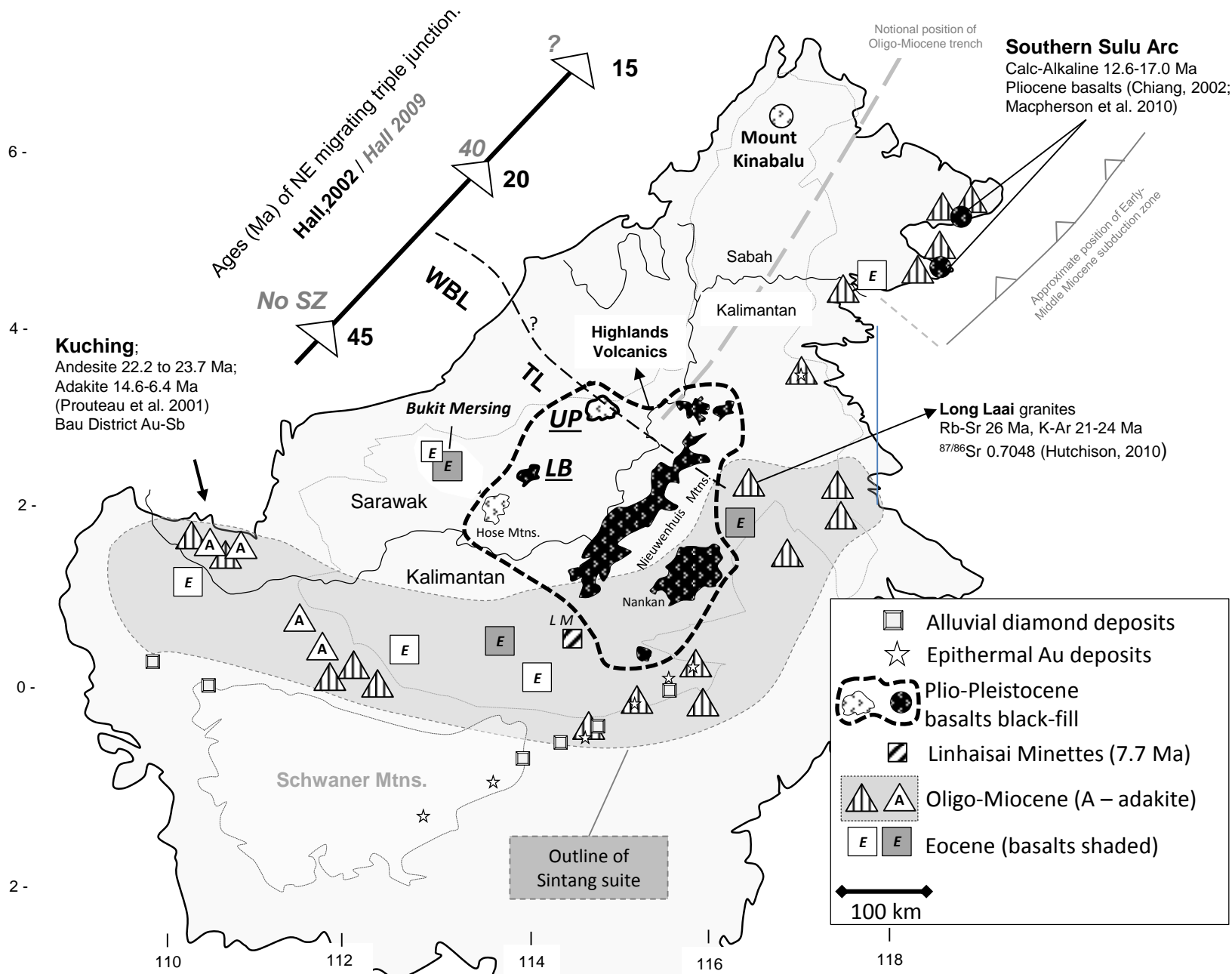


Figure 3

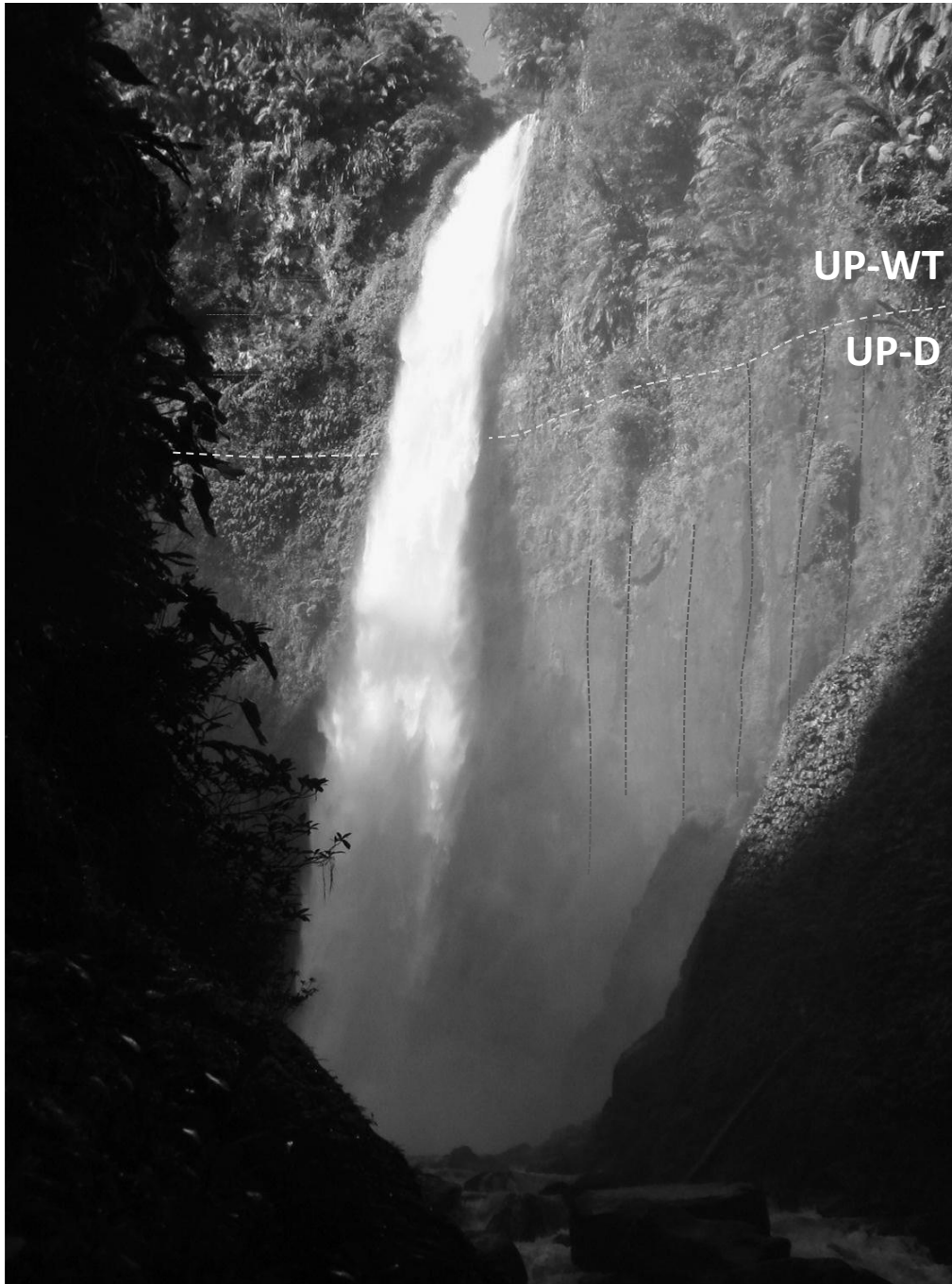


Figure 4

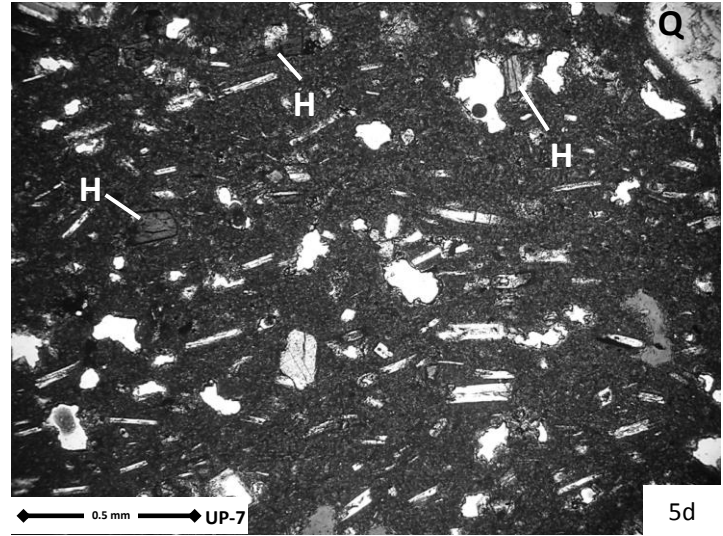
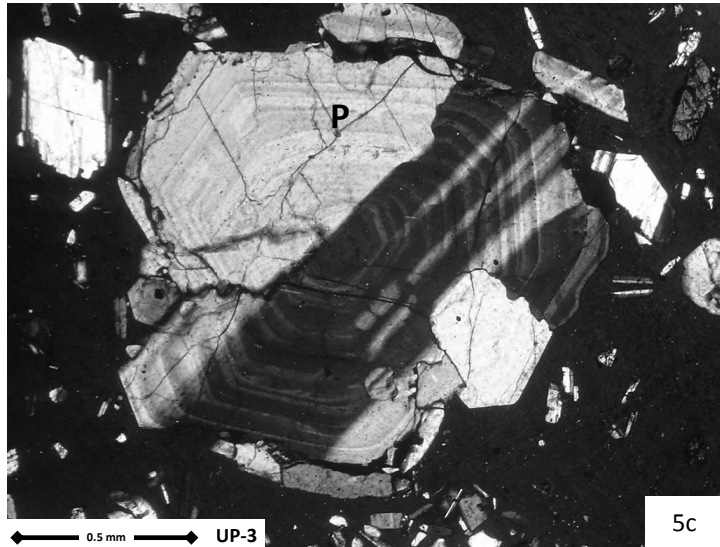
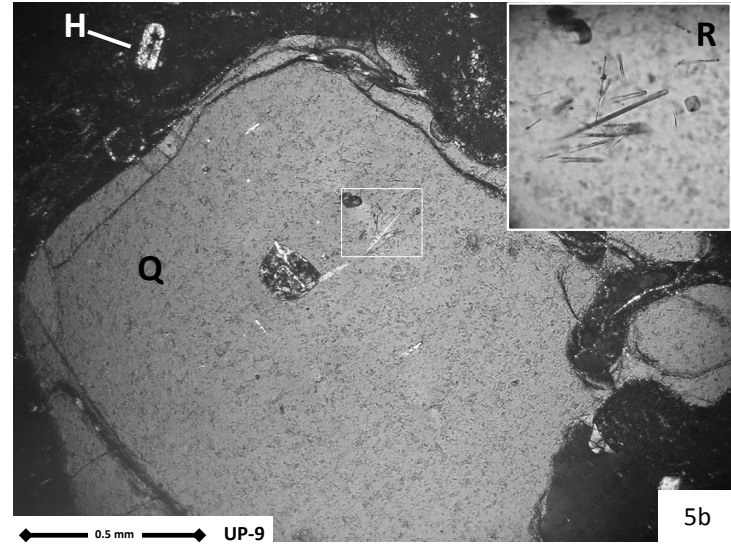
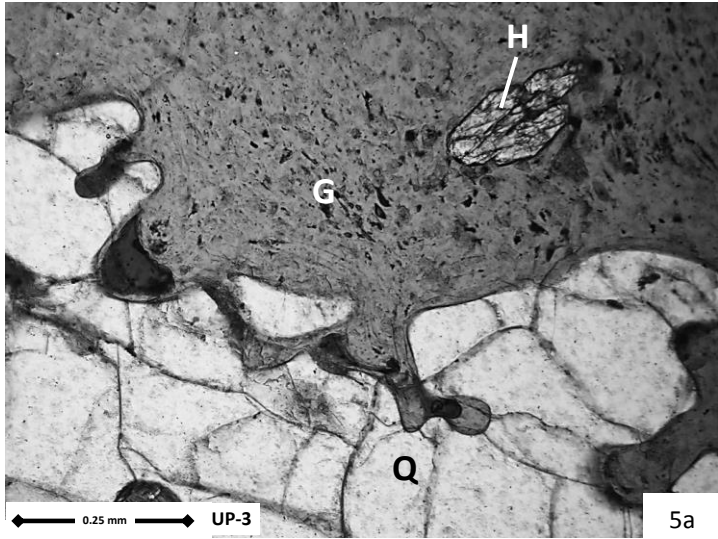


Figure 5

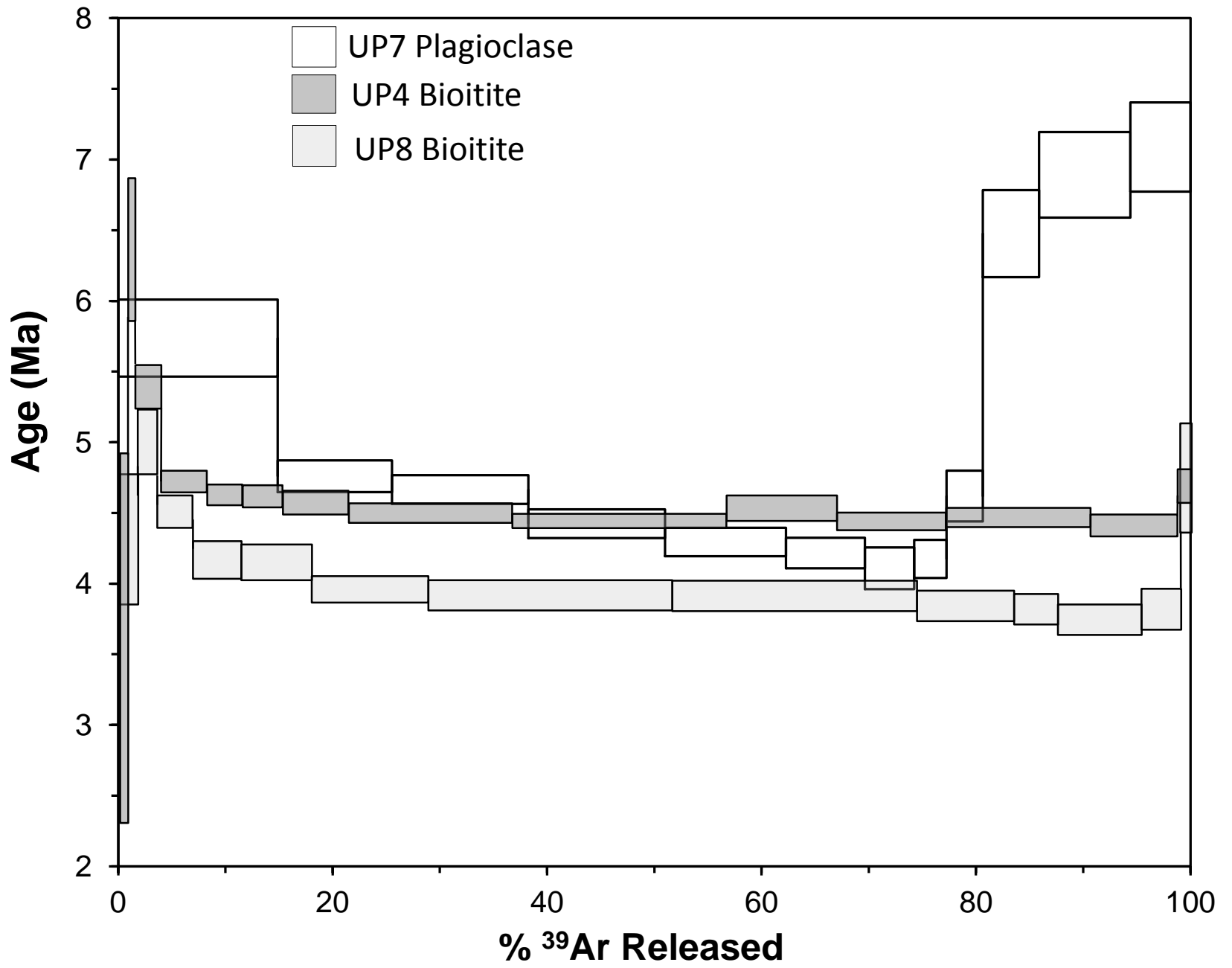


Figure 6

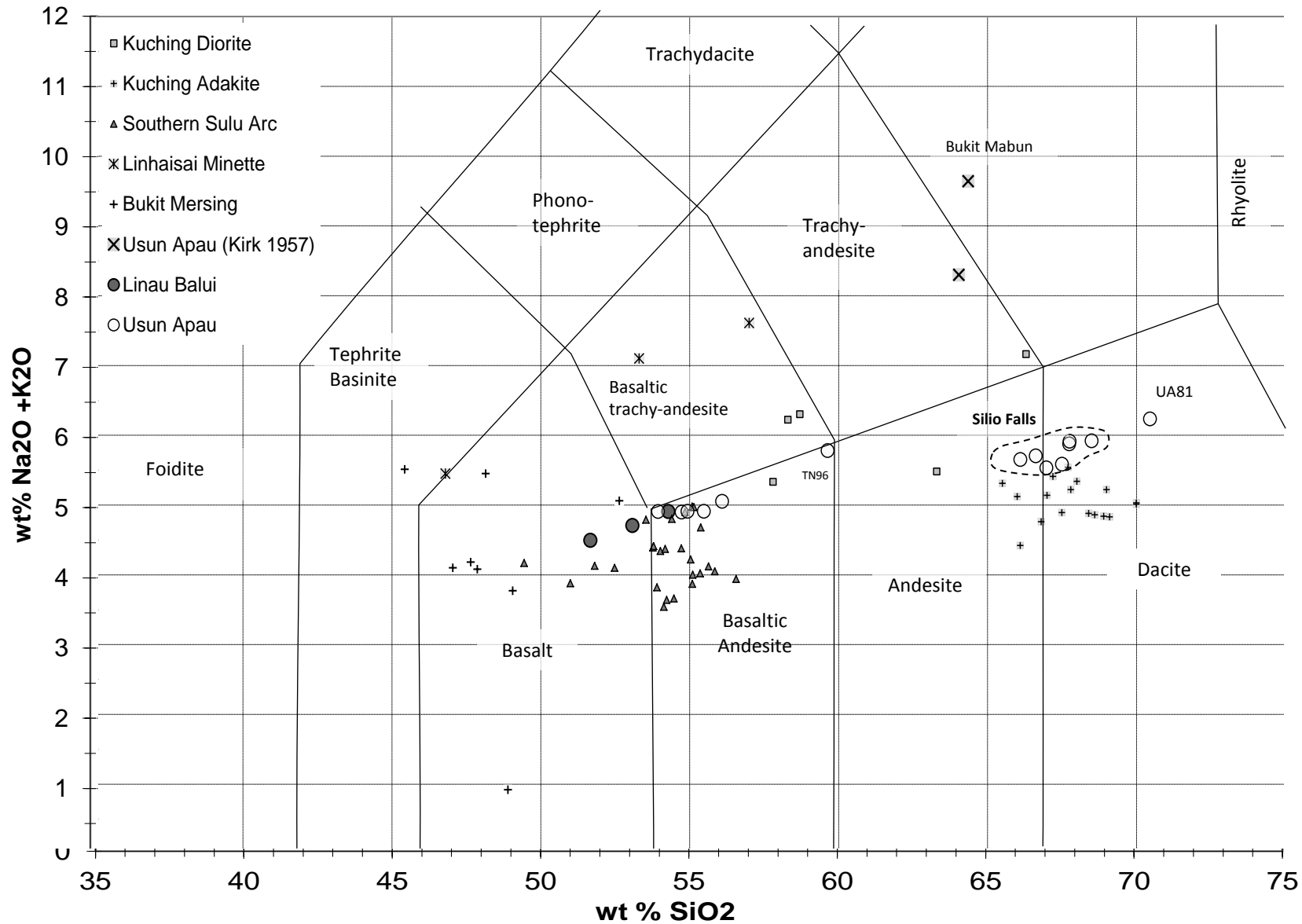


Figure 7

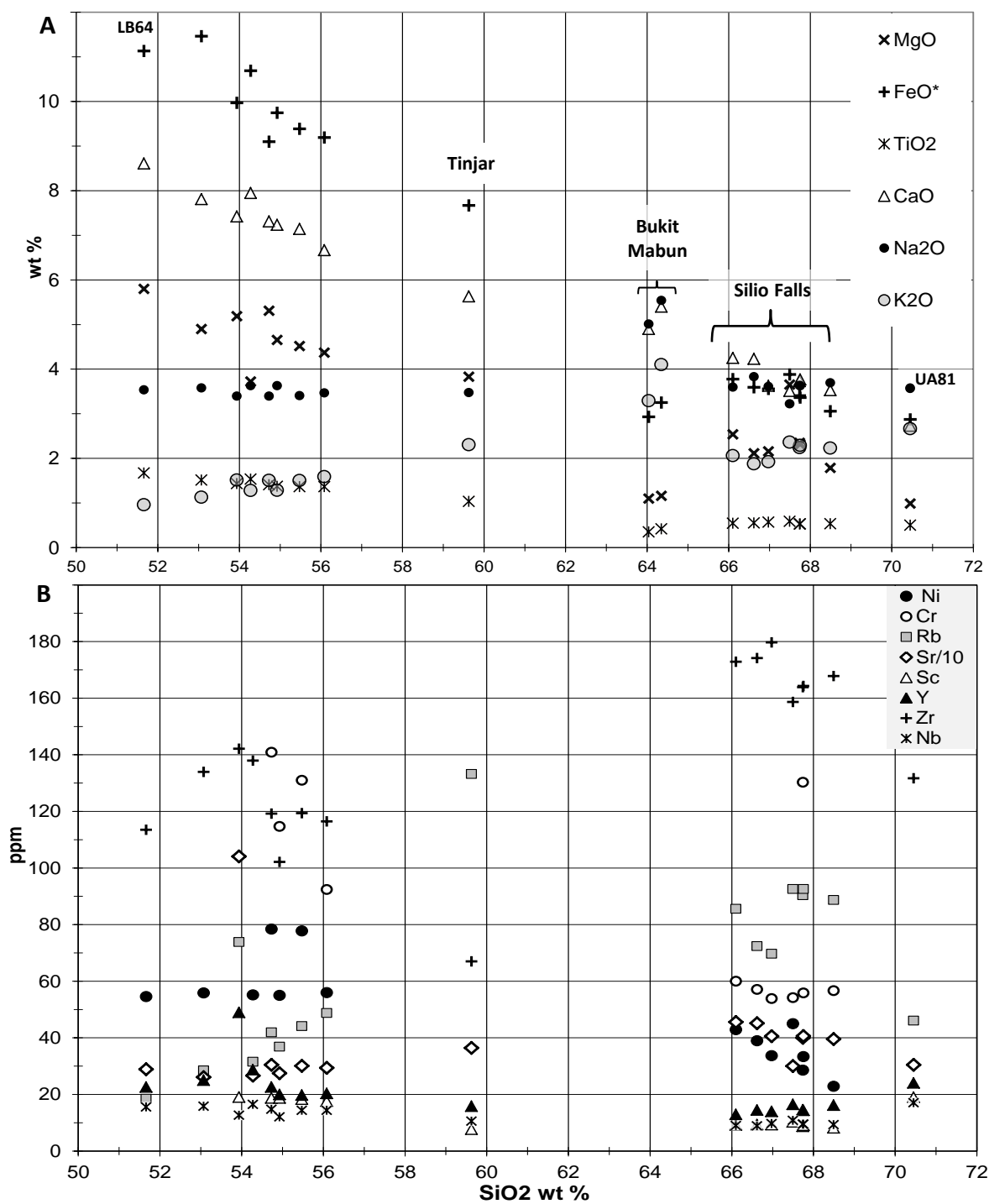


Figure 8

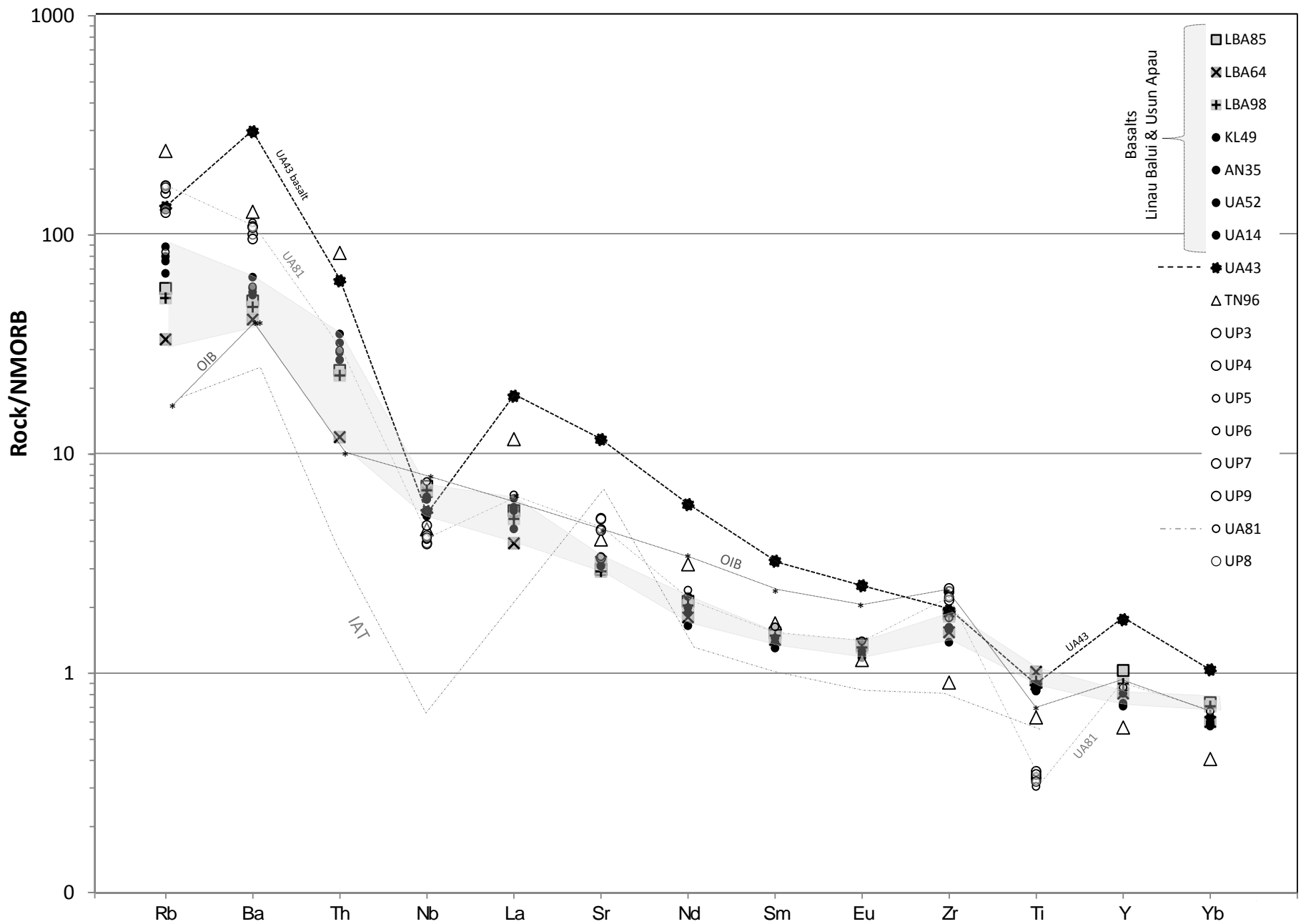


Figure 9

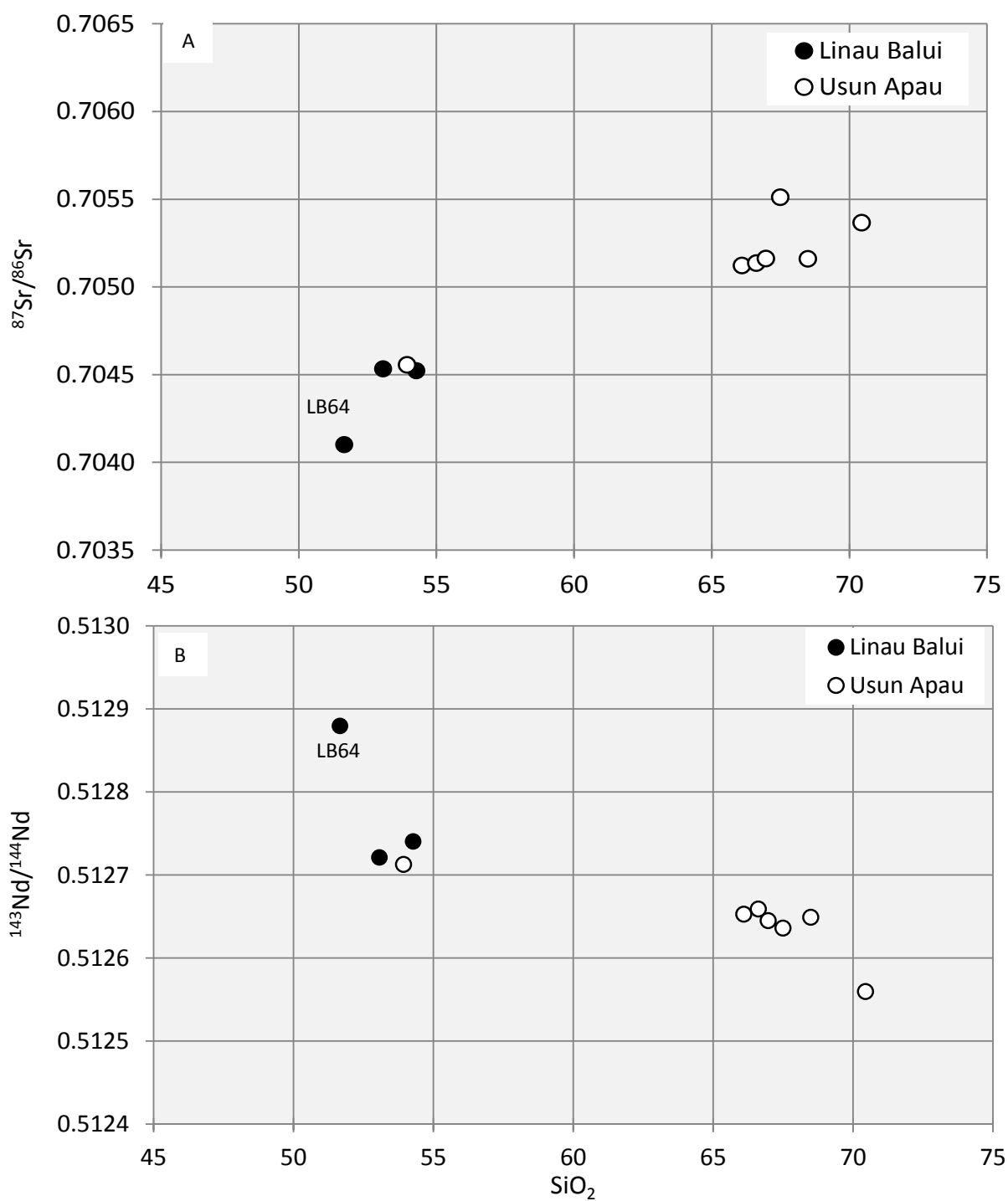


Figure 10

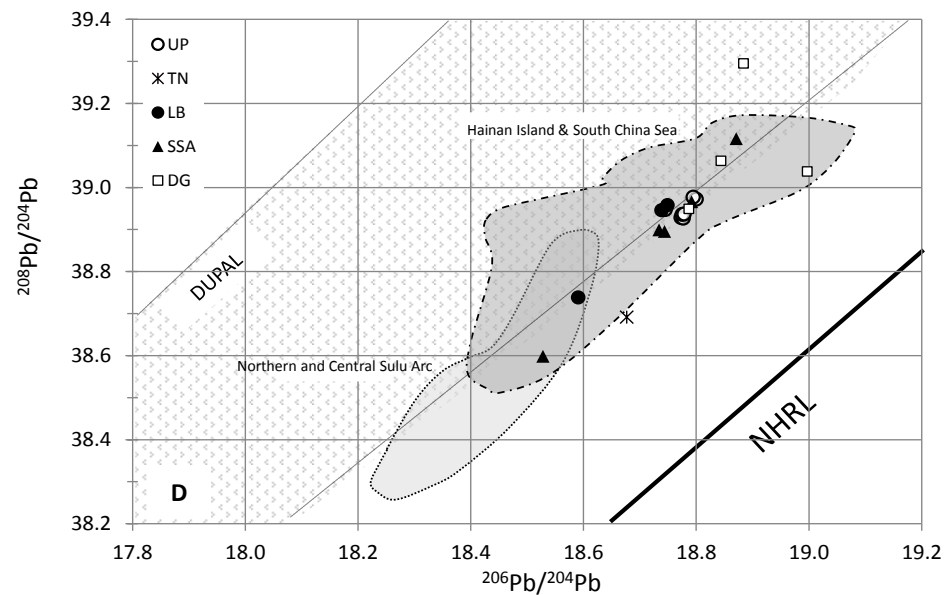
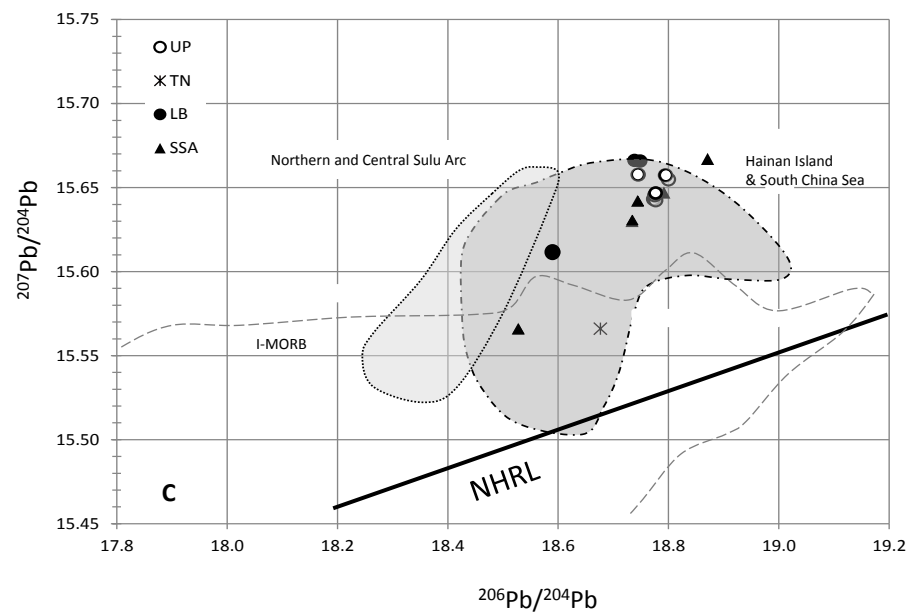
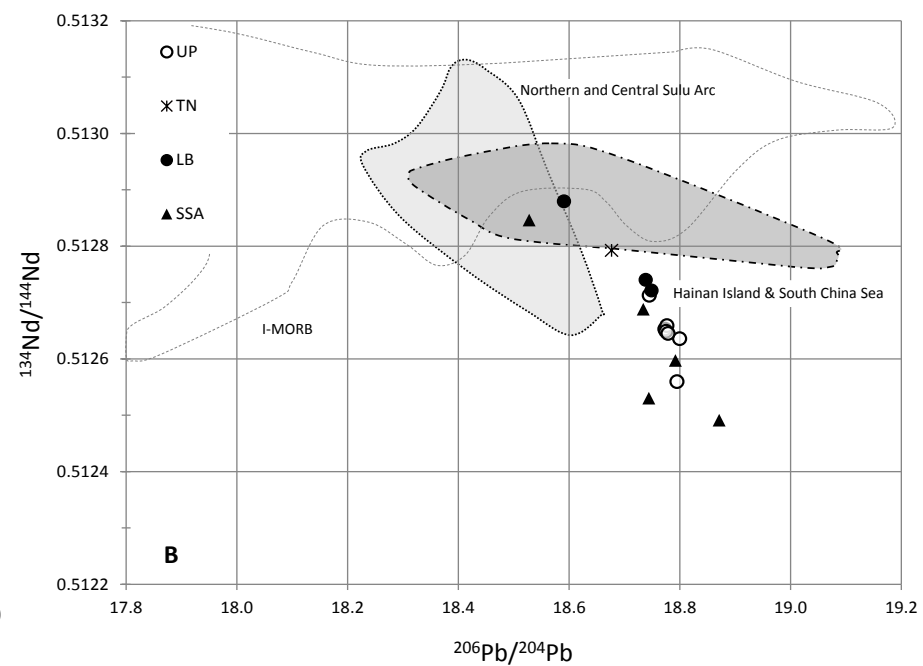
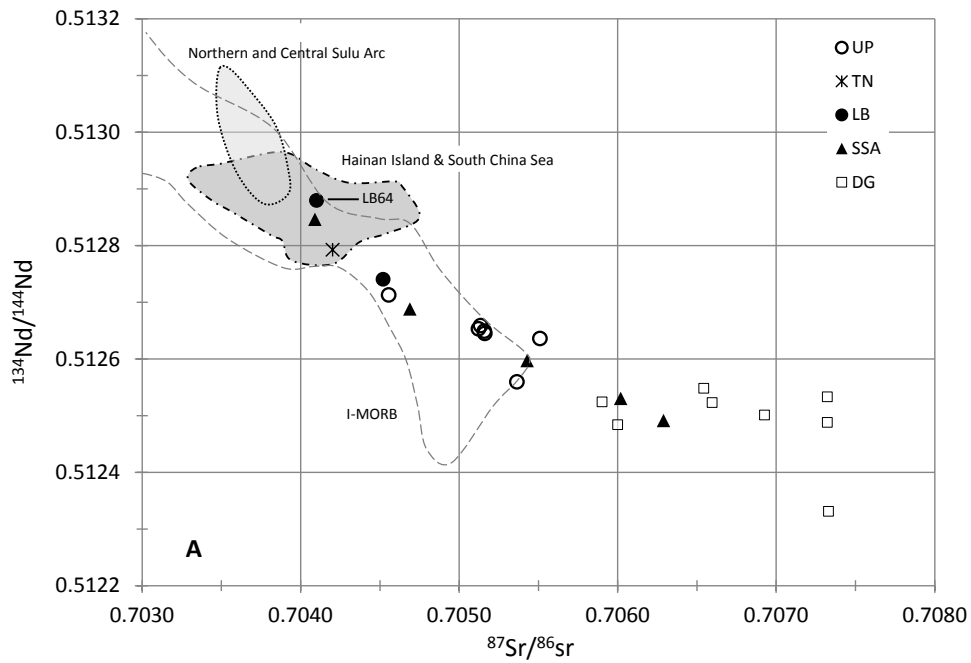


Figure 11

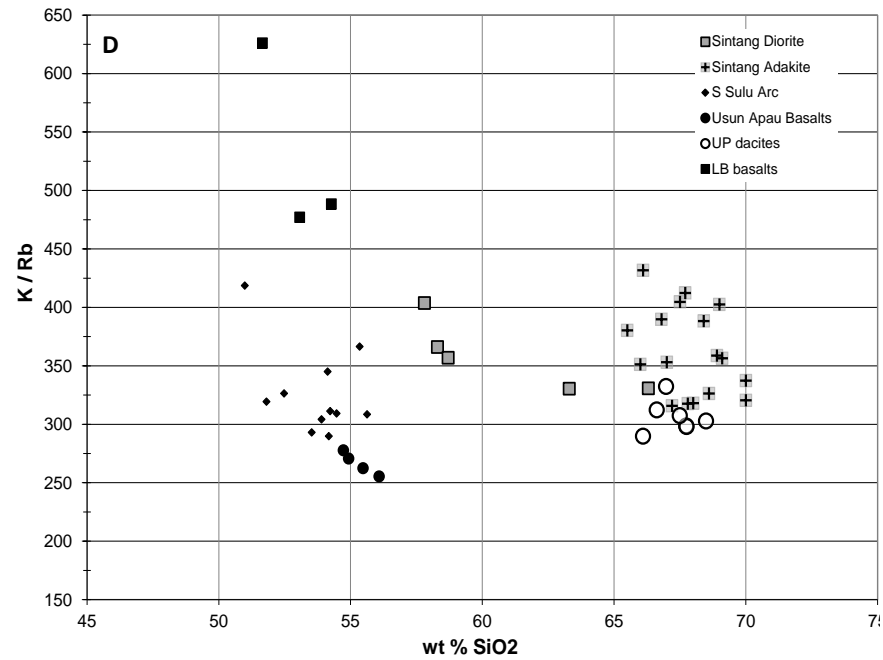
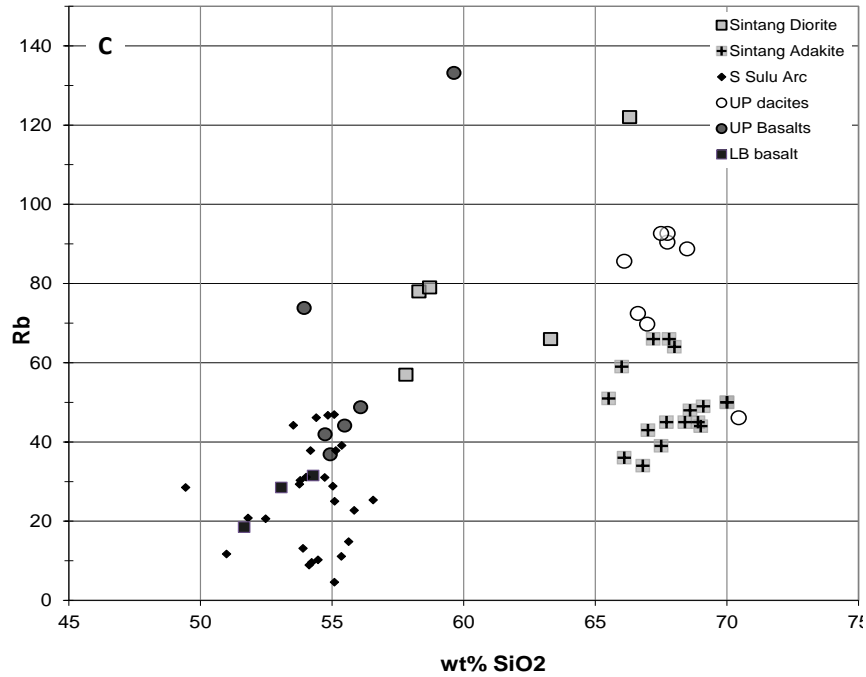
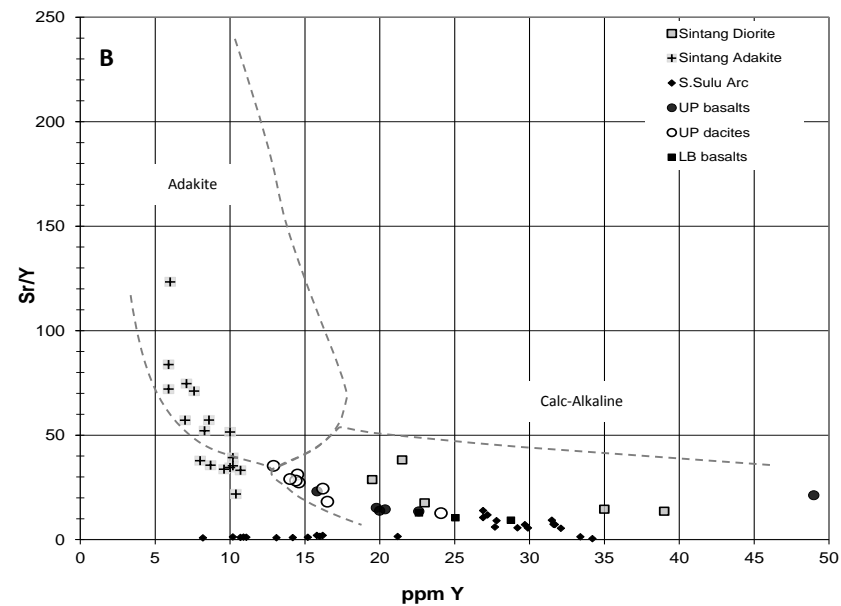
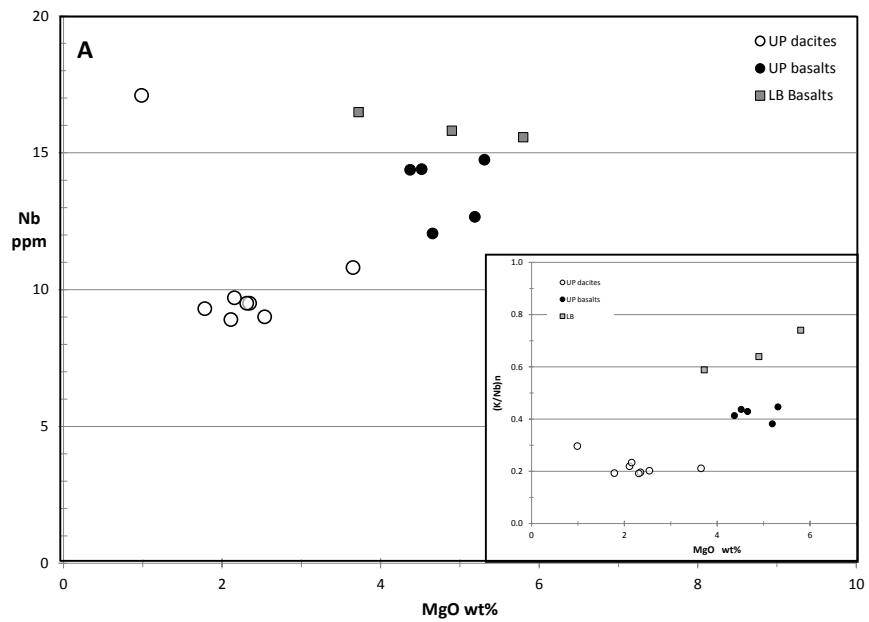


Figure 12

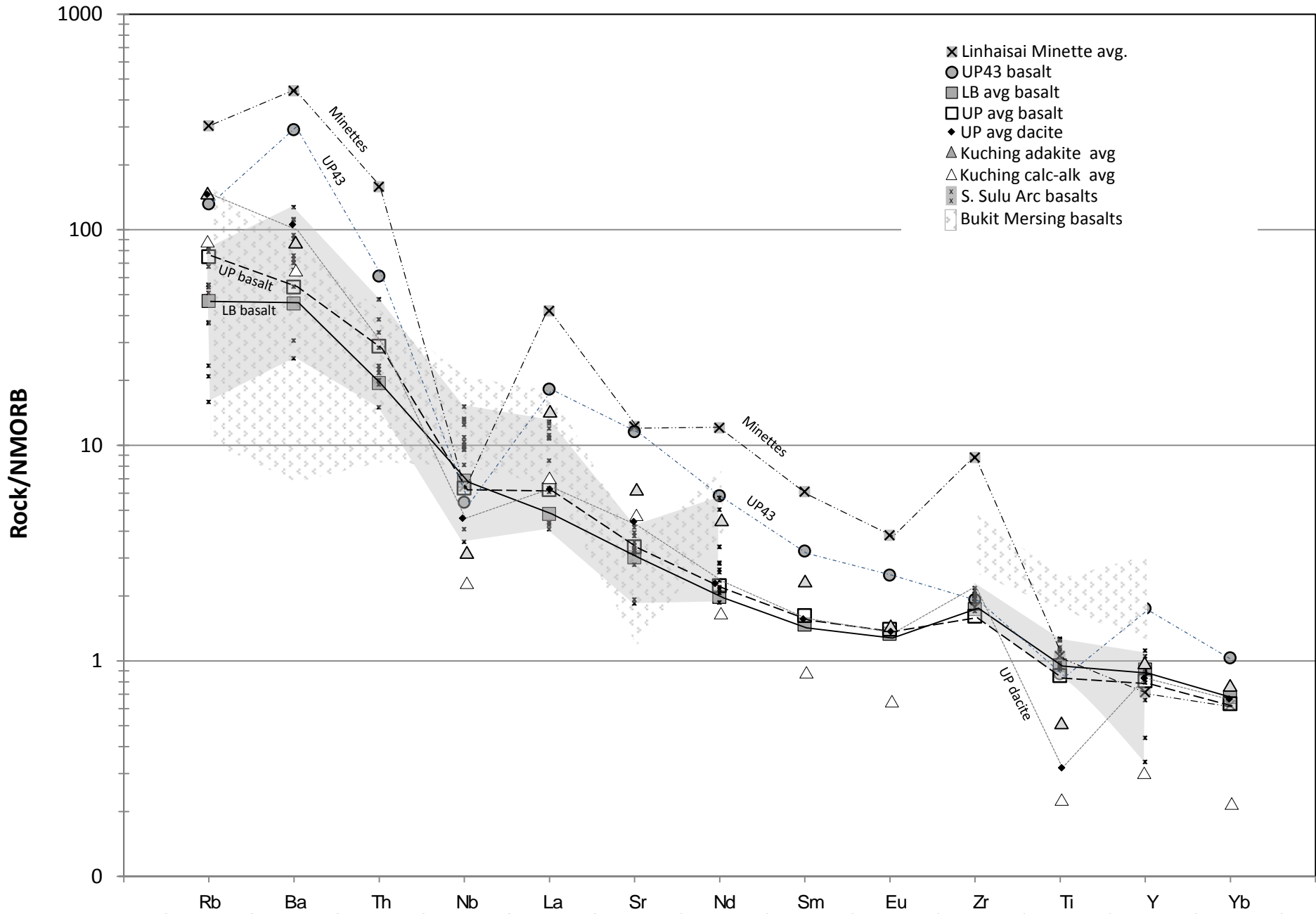


Figure 12

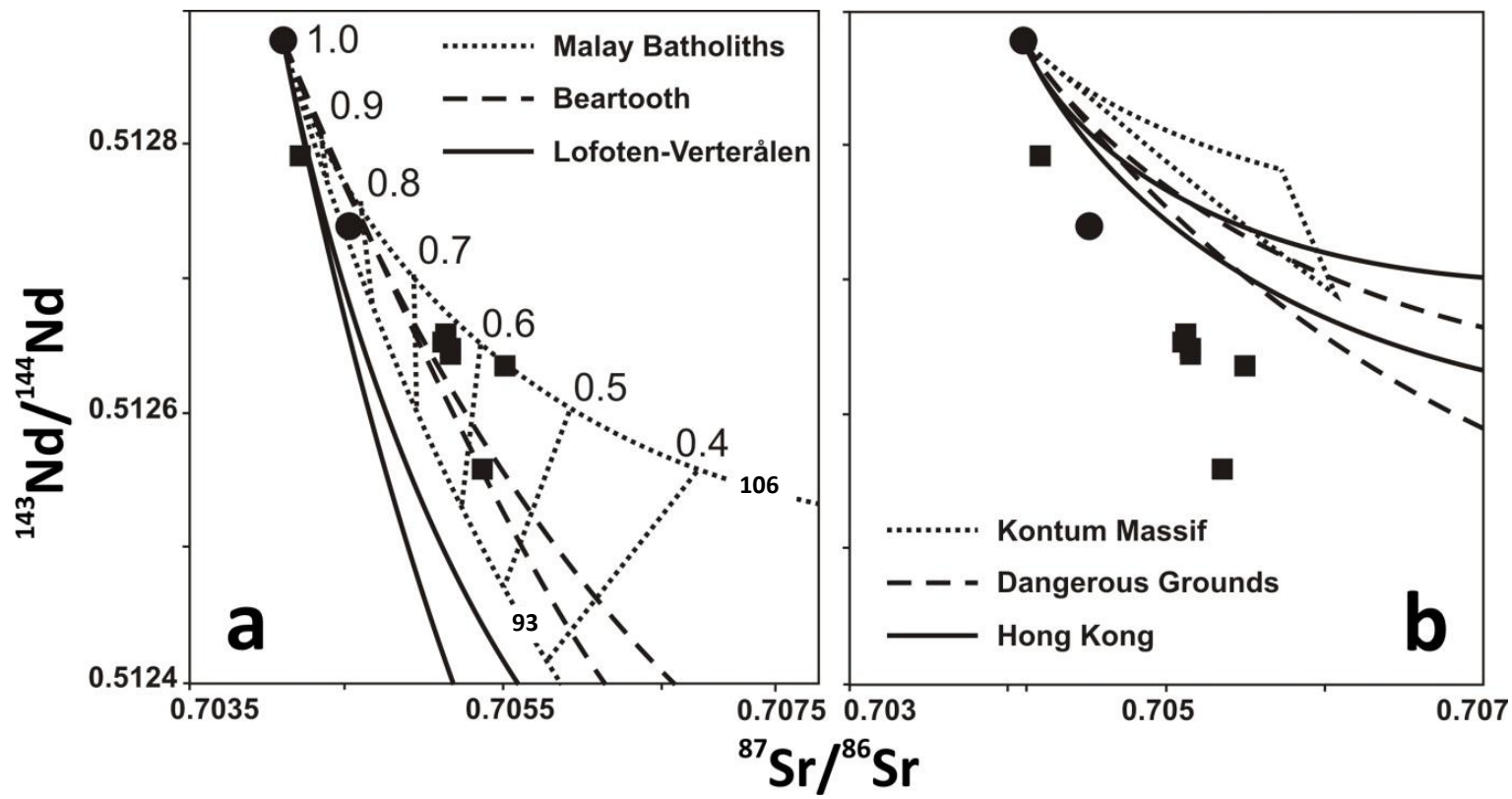


Figure 14

UP4: Andesite-Biotite, 11.80 mg, J = 0.001580 ± 0.59%

step	T (C)	t (min.)	36Ar	37Ar	38Ar	39Ar	40Ar	%40Ar*	% 39Ar rIsd	Ca/K	40Ar*/39 ArK	Age (Ma)	1s.d.
1	650	12	4.846	3.448	1.185	12.075	1381.58	0.6	1.0	0.943909	0.666563	1.90	1.27
2	725	12	1.297	4.154	0.422	8.255	384.301	4.9	0.7	1.663759	2.163354	6.16	0.31
3	790	12	1.093	5.607	0.788	28.377	358.384	14.7	2.3	0.653096	1.759361	5.01	0.09
4	850	12	0.437	4.995	1.124	50.301	197.358	42.0	4.1	0.328194	1.483612	4.22	0.05
5	900	12	0.331	3.665	0.886	40.390	151.006	44.5	3.3	0.299895	1.439306	4.10	0.05
6	950	12	0.388	2.588	1.047	47.544	178.074	43.7	3.9	0.179896	1.438603	4.10	0.05
7	1000	12	0.556	1.781	1.657	75.984	264.970	44.1	6.2	0.077461	1.416099	4.03	0.05
8	1040	12	0.979	1.204	3.976	187.271	537.285	50.1	15.2	0.021247	1.387971	3.95	0.05
9	1070	12	0.839	0.874	5.187	247.004	575.287	60.5	20.0	0.011693	1.366173	3.89	0.04
10	1090	12	0.391	0.668	2.739	130.556	292.479	66.8	10.6	0.016909	1.391487	3.96	0.05
11	1120	12	0.304	0.872	2.570	121.423	251.759	72.0	9.9	0.023733	1.363360	3.88	0.04
12	1160	12	0.269	1.905	3.487	165.381	302.453	80.5	13.4	0.038067	1.367931	3.90	0.04
13	1215	12	0.180	2.124	2.130	100.804	186.929	82.7	8.2	0.069633	1.348946	3.84	0.04
14	1400	12	0.155	1.767	0.390	17.054	67.650	74.0	1.4	0.342440	1.447393	4.12	0.07

Total gas age = 3.96 0.03

Steps 8-13 Plateau age = 3.90 0.04

UP7: Dacite-Plagioclase, 24.68 mg, J = 0.001635 ± 0.69%

step	T (C)	t (min.)	36Ar	37Ar	38Ar	39Ar	40Ar	%40Ar*	% 39Ar rIsd	Ca/K	40Ar*/39 ArK	Age (Ma)	1s.d.
1	600	12	9.122	51.242	4.027	141.252	2853.28	9.6	14.9	1.174744	1.948062	5.74	0.14
2	640	12	1.011	29.476	1.568	101.188	446.574	37.7	10.7	0.943240	1.615873	4.76	0.06
3	680	12	0.743	35.317	1.728	120.701	397.662	49.8	12.7	0.947450	1.583581	4.67	0.05
4	720	12	0.578	36.476	1.723	120.984	340.901	56.3	12.7	0.976261	1.501671	4.42	0.05
5	770	12	0.493	34.620	1.526	106.960	291.288	57.2	11.3	1.048097	1.457492	4.29	0.05
6	830	12	0.466	31.984	1.073	69.876	227.971	47.9	7.4	1.482366	1.430986	4.22	0.05
7	900	12	0.378	23.637	0.723	43.449	164.627	41.9	4.6	1.761971	1.394287	4.11	0.07
8	990	12	0.429	16.084	0.504	28.684	160.479	29.3	3.0	1.816132	1.417053	4.18	0.07
9	1090	12	1.039	16.534	0.723	32.136	342.947	15.6	3.4	1.666327	1.568286	4.62	0.09
10	1180	12	3.196	20.858	1.400	49.885	1012.63	11.0	5.3	1.354058	2.199788	6.48	0.15
11	1260	12	5.845	31.728	2.389	80.686	1840.74	10.3	8.5	1.273412	2.341004	6.89	0.15
12	1400	12	3.736	28.766	1.557	53.240	1182.22	11.0	5.6	1.749952	2.408051	7.09	0.16

Total gas age = 5.11 0.05

No plateau

No isochron

UP8: Dacite-Biotite, 8.90 mg, J = 0.00152 ± 0.93%

step	T (C)	t (min.)	36Ar	37Ar	38Ar	39Ar	40Ar	%40Ar*	% 39Ar rIsd	Ca/K	40Ar*/39 ArK	Age (Ma)	1s.d.
1	730	12	1.885	16.062	0.671	14.138	553.797	4.1	2.1	3.782874	1.559721	4.27	0.23
2	800	12	0.353	12.167	0.306	11.736	119.372	21.5	1.7	3.451690	1.811623	4.96	0.11
3	860	12	0.276	9.402	0.503	22.300	112.978	39.4	3.3	1.402894	1.631004	4.47	0.06
4	920	12	0.318	7.185	0.656	29.125	113.242	39.5	4.3	0.820723	1.508548	4.13	0.07
5	970	12	0.356	4.081	0.981	46.958	170.899	47.3	6.9	0.289085	1.501238	4.11	0.06
6	1010	12	0.395	2.053	1.490	72.577	215.676	53.5	10.7	0.094088	1.432161	3.92	0.05
7	1040	12	0.682	1.464	3.186	154.238	411.703	55.7	22.7	0.031571	1.417177	3.88	0.05
8	1070	12	0.540	1.219	3.131	156.065	374.564	62.5	23.0	0.025980	1.416446	3.88	0.05
9	1100	12	0.253	0.957	1.204	60.404	155.342	62.8	8.9	0.052697	1.387210	3.80	0.05
10	1130	12	0.155	0.743	0.557	26.473	80.626	64.3	3.9	0.093353	1.385749	3.80	0.05
11	1170	12	0.199	1.153	1.087	52.899	127.995	68.3	7.8	0.072497	1.353591	3.71	0.05
12	1220	12	0.119	1.530	0.532	25.747	69.315	78.2	3.8	0.197661	1.385018	3.79	0.07
13	1400	12	0.128	1.712	0.131	5.531	45.640	43.7	0.8	1.029822	1.716188	4.70	0.19

Total gas age = 3.94 0.04

Steps 6-10 Plateau age = 3.86 0.05

Steps 6-8 Isochron age = 3.84 0.06

% 39Ar rIsd (released)

4 amu discrimination = 1.0433 ± 0.20%, 40/39K = 0.0148 ± 79.07%, 36/37Ca = 0.00026 ± 3.15%, 39/37Ca = 0.00067 ± 1.70%

note: isotope beams in mV, rIsd = released, error in age includes J error, all errors 1 sigma

(36Ar through 40Ar are measured beam intensities, corrected for decay for the age calculations)

K concentration is not measured directly in the ⁴⁰Ar/³⁹Ar method.

Measurement of ³⁹Ar indirectly gives the ⁴⁰K via the irradiation and calibration with the fluence monitor standard.

Location	UP3 2.85N 114.71E	UP4 2.85N 114.71E	UP5 2.85N 114.71E	UP6 2.85N 114.71E	UP7 2.85N 114.71E	UP8 2.85N 114.71E	UP9 2.85N 114.71E	UA81 2.931N 114.58	UA43 2.94N 114.62E	UA52 2.95N 114.63E Basaltic	UA14 2.95N 114.67E Basaltic	TN96 3.24N 114.35E Basaltic	LB98 2.46N 114.10E	LB64 2.42N 114.07E	LB85 2.43N 114.08E Basaltic	KL49 3.04N 114.65E Basaltic	AN35 2.99N 114.86E Basaltic
wt%	Andesite	Andesite	Dacite	Dacite	Dacite	Dacite	Andesite	Dacite	Basalt	Andesite	Andesite	Andesite	Basalt	Basalt	Andesite	Andesite	Andesite
SiO2	66.10	66.62	68.49	67.75	67.50	67.74	66.97	70.45	53.94	54.73	55.48	59.63	53.07	51.66	54.28	56.08	54.93
TiO2	0.54	0.55	0.53	0.53	0.59	0.53	0.57	0.50	1.44	1.41	1.37	1.04	1.51	1.67	1.53	1.37	1.37
Al2O3	16.94	17.01	16.52	16.17	15.10	16.18	17.41	16.10	16.90	16.88	16.82	16.10	16.17	16.25	16.50	16.93	16.81
FeO*	3.78	3.59	3.06	3.36	3.88	3.41	3.56	2.87	9.97	9.10	9.39	7.67	11.46	11.13	10.69	9.19	9.75
MnO	0.07	0.06	0.05	0.07	0.07	0.07	0.06	0.03	0.00	0.13	0.14	0.09	0.13	0.11	0.16	0.13	0.14
MgO	2.54	2.11	1.78	2.31	3.65	2.35	2.16	0.99	5.19	5.31	4.52	3.83	4.90	5.80	3.72	4.37	4.66
CaO	4.25	4.23	3.53	3.77	3.51	3.73	3.63	2.73	7.42	7.31	7.14	5.63	7.81	8.61	7.95	6.67	7.23
Na2O	3.60	3.83	3.69	3.63	3.22	3.64	3.61	3.57	3.40	3.39	3.41	3.48	3.58	3.54	3.63	3.47	3.63
K2O	2.06	1.88	2.23	2.29	2.36	2.24	1.92	2.67	1.51	1.51	1.50	2.31	1.13	0.96	1.28	1.59	1.28
P2O5	0.12	0.12	0.11	0.12	0.12	0.12	0.10	0.11	0.24	0.23	0.24	0.24	0.24	0.27	0.26	0.22	0.20
LOI	1.51	3.09	2.56	1.78	1.95	2.51	2.53	2.97	0.66	0.57	1.84	3.37	0.98	1.55	1.83	1.74	2.05
ppm																	
Ni	42.9	39.0	22.9	33.4	45.0	28.6	33.7	NA	NA	78.4	77.8	NA	NA	NA	NA	55.9	54.6
Cr	60.0	57.1	53.9	54.2	130.3	55.9	56.7	NA	NA	140.9	131.0	NA	NA	NA	NA	92.4	114.7
Sc	9.2	9.3	8.2	9.1	10.3	8.7	9.3	19.0	19.0	18.7	18.3	7.7	21.0	20.6	22.5	17.6	18.8
V	64.1	55.0	55.1	56.5	70.2	56.9	56.3	NA	NA	122.4	115.2	NA	NA	NA	NA	115.2	122.5
Ba	337.5	321.4	362.7	379.8	365.6	361.3	365.8	194.7	989.5	184.1	191.6	427.4	157.6	138.3	167.7	215.1	178.3
Rb	85.6	72.4	88.7	92.6	92.6	90.4	69.7	46.1	73.8	41.9	44.1	133.2	28.5	18.5	31.5	48.8	36.9
Sr	456.0	451.5	395.7	406.5	300.3	400.0	405.8	304.8	1040.7	304.6	300.7	364.4	261.2	288.8	266.3	294.0	275.2
Zr	172.9	174.2	167.8	164.3	158.7	163.9	179.7	131.7	142.1	119.2	119.4	67.0	134.0	113.5	138.0	116.5	102.1
Y	12.9	14.5	16.2	14.4	16.5	14.6	14.0	24.1	49.0	22.6	19.8	15.8	25.1	22.6	28.8	20.4	20.0
Nb	9.0	8.9	9.3	9.5	10.8	9.5	9.7	17.1	12.7	14.7	14.4	10.5	15.8	15.6	16.5	14.4	12.1
Ga	17.0	15.7	16.2	17.2	16.1	17.0	16.7	NA	NA	18.1	19.5	NA	NA	NA	NA	19.7	19.6
Cu	17.7	22.6	15.3	18.2	14.5	17.3	33.1	NA	NA	49.1	49.3	NA	NA	NA	NA	47.4	50.8
Zn	60.4	60.3	48.2	60.4	52.5	58.3	62.4	NA	NA	94.2	93.6	NA	NA	NA	NA	90.3	98.1
Pb	9.3	10.4	12.0	11.2	9.4	11.4	12.0	5.1	23.2	4.1	4.6	23.0	4.5	1.7	4.7	5.3	4.1
La	NA	NA	NA	NA	NA	NA	NA	16.1	45.5	15.6	14.2	29.0	12.6	9.7	13.7	13.7	11.3
Ce	NA	NA	NA	NA	NA	NA	NA	32.3	89.1	30.2	27.6	56.7	26.3	21.3	27.7	26.1	21.9
Pr	NA	NA	NA	NA	NA	NA	NA	4.09	10.4	3.9	3.5	6.2	3.4	2.8	3.5	3.3	2.8
Nd	NA	NA	NA	NA	NA	NA	NA	17.4	42.6	16.3	14.5	22.8	14.8	13.1	15.5	13.7	12.0
Sm	NA	NA	NA	NA	NA	NA	NA	4.26	8.49	4.26	3.79	4.43	3.89	3.72	4.00	3.62	3.41
Eu	NA	NA	NA	NA	NA	NA	NA	1.43	2.55	1.43	1.28	1.17	1.33	1.39	1.37	1.23	1.20
Gd	NA	NA	NA	NA	NA	NA	NA	4.57	8.65	4.61	4.02	3.72	4.41	4.25	4.65	3.98	3.84
Tb	NA	NA	NA	NA	NA	NA	NA	0.73	1.23	0.75	0.67	0.55	0.72	0.70	0.76	0.67	0.65
Dy	NA	NA	NA	NA	NA	NA	NA	4.32	7.02	4.50	4.02	2.98	4.31	4.11	4.59	4.05	3.96
Ho	NA	NA	NA	NA	NA	NA	NA	0.83	1.37	0.89	0.79	0.54	0.85	0.78	0.92	0.80	0.79
Er	NA	NA	NA	NA	NA	NA	NA	2.32	3.85	2.30	2.07	1.46	2.38	2.15	2.58	2.14	2.11
Tm	NA	NA	NA	NA	NA	NA	NA	0.33	0.52	0.32	0.29	0.20	0.34	0.29	0.36	0.30	0.29
Yb	NA	NA	NA	NA	NA	NA	NA	2.04	3.15	1.93	1.75	1.24	2.15	1.83	2.23	1.83	1.79
Lu	NA	NA	NA	NA	NA	NA	NA	0.29	0.47	0.30	0.27	0.17	0.31	0.26	0.33	0.29	0.28
Th	NA	NA	NA	NA	NA	NA	NA	3.53	7.32	3.46	3.82	9.81	2.72	1.42	2.86	4.19	3.19
Hf	NA	NA	NA	NA	NA	NA	NA	3.04	3.65	3.02	3.11	1.87	3.09	2.63	3.16	3.05	2.72
Ta	NA	NA	NA	NA	NA	NA	NA	1.02	0.97	0.93	0.92	0.92	0.90	0.85	0.95	0.98	0.79
U	NA	NA	NA	NA	NA	NA	NA	0.73	1.96	0.85	0.95	2.25	0.55	0.37	0.60	1.16	0.84
Cs	NA	NA	NA	NA	NA	NA	NA	2.01	2.57	1.81	2.00	5.47	1.20	0.43	1.49	2.43	1.67

LOI Loss on Ignition
NA No Analysis

Sample	Lithology	$^{87}\text{Sr}/^{86}\text{Sr}$	$^{143}\text{Nd}/^{144}\text{Nd}$	$^{206}\text{Pb}/^{204}\text{Pb}$	$^{207}\text{Pb}/^{204}\text{Pb}$	$^{208}\text{Pb}/^{204}\text{Pb}$
UP3	Andesite	0.705122	0.512653	18.773	15.643	38.929
UP4	Andesite	0.705135	0.512659	18.777	15.642	38.927
UP5	Dacite	0.705159	0.512649	18.775	15.645	38.936
UP7	Dacite	0.705511	0.512636	18.800	15.655	38.972
UP9	Andesite	0.705161	0.512645	18.779	15.646	38.937
UA43	Basalt	0.704555	0.512713	18.745	15.658	38.947
UA81	Dacite	0.705365	0.512559	18.795	15.657	38.977
TN96	Andesite	0.704204	0.512792	18.677	15.566	38.691
LBA64	Basalt	0.704100	0.512879	18.591	15.612	38.738
LBA85	Basalt	0.704521	0.512740	18.739	15.666	38.946
LBA98	Basalt	0.704533	0.512721	18.749	15.666	38.958